RL-TR-97-154
In-House Report
October 1997
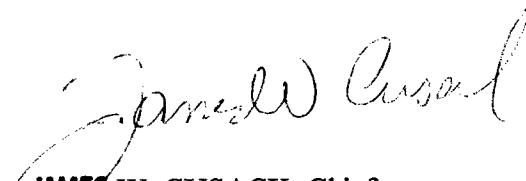
AN OVERVIEW OF THE CREST CHALLENGE

19980402 133

Rome Laboratory
rce Materiel Command
Rome, New York

DTIC QUALITY INSPECTED 3

This report has been reviewed by the Rome Laboratory Public Affairs Office (PA) and is releasable to the National Technical Information Service (NTIS). At NTIS it will be releasable to the general public, including foreign nations.
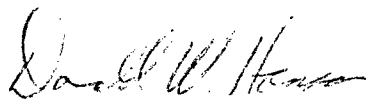
RL-TR-97-154 has been reviewed and is approved for publication.

APPROVED:

JAMES W. CUSACK, Chief
Surveillance Division
Surveillance & Photonics Directorate

FOR THE DIRECTOR:

DONALD W. HANSON, Director
Surveillance & Photonics Directorate

REPORT DOCUMENTATION PAGE

Public reporting burden for this collection of information is estimated to average 1 hour per response, including the time for reviewing instructions, searching existing data sources, gathering and maintaining the data needed, and completing and reviewing the collection of information. Send comments regarding this burden estimate or any other aspect of this collection of information, including suggestions for reducing this burden, to Washington Headquarters Services, Directorate for Information Operations and Reports, 1215 Jefferson Davis Highway, Suite 1204, Arlington, VA 22202-4302, and to the Office of Management and Budget, Paperwork Reduction Project (0704-0188), Washington, DC 20503.

1. AGENCY USE ONLY (Leave blank)	2. REPORT DATE	3. REPORT TYPE AND DATES COVERED
	October 1997	In-House, Mar 96 - Dec 96

4. TITLE AND SUBTITLE

AN OVERVIEW OF THE CREST CHALLENGE

5. FUNDING NUMBERS

PE - 63762E
PR - MSEF
TA - PR
WU- OJ

6. AUTHOR(S)

Peter A. Zulch

7. PERFORMING ORGANIZATION NAME(S) AND ADDRESS(ES)

Rome Laboratory/OCSA
26 Electronic Pky
Rome, NY 13441-4514

8. PERFORMING ORGANIZATION REPORT NUMBER

RL-TR-97-154

9. SPONSORING/MONITORING AGENCY NAME(S) AND ADDRESS(ES)

Rome Laboratory/OCSA
26 Electronic Pky
Rome, NY 13441-4514

Advanced Research Projects Agency
3701 North Fairfax Drive
Arlington, VA 22203-1714

10. SPONSORING/MONITORING AGENCY REPORT NUMBER

RL-TR-97-154

11. SUPPLEMENTARY NOTES

Rome Laboratory Project Engineer: Peter A. Zulch/OCSA, (315)330-7861.

12a. DISTRIBUTION AVAILABILITY STATEMENT

Approved for public release; distribution unlimited.

12b. DISTRIBUTION CODE

13. ABSTRACT (Maximum 200 words)

In support of the Defense Advanced Research Projects Agency Advanced Signal Processing Program and the Common Research Environment for Space Time Adaptive Processing (STAP) Technology (CREST), a challenge had been issued to the radar and signal processing community. Several simulated data sets that emulate returns from a flying phased array surveillance radar were created and placed on the World Wide Web. The challenge was to resolve all target information. Each of the four data sets for the challenge was created with the Rome Laboratory Space Time Adaptive Processing Algorithm Development Tool. This report documents the generation and properties of each data set contained in the CREST challenge. Also, several performance results using conventional and Space Time Adaptive Processing techniques are given to indicate the presence of targets in each data set.

14. SUBJECT TERMS

space time adaptive processing (STAP), airborne early warning (AEW) radar, surveillance radar, phased arrays

15. NUMBER OF PAGES

134

16. PRICE CODE

17. SECURITY CLASSIFICATION OF REPORT	18. SECURITY CLASSIFICATION OF THIS PAGE	19. SECURITY CLASSIFICATION OF ABSTRACT	20. LIMITATION OF ABSTRACT
UNCLASSIFIED	UNCLASSIFIED	UNCLASSIFIED	UL

Abstract

In support of the Defense Advanced Research Projects Agency Advanced Signal Processing program a challenge had been issued to the radar and signal processing community. Several simulated data sets that emulate returns from a flying phased array surveillance radar were created and placed on the World Wide Web. The challenge was to resolve all target information. Each of the four data sets for the challenge was created with the Rome Laboratory Space Time Adaptive Processing Algorithm Development Tool. This report documents the generation and properties of each data set contained in the CREST Challenge. Also, several performance results using conventional and Space-Time Adaptive Processing (STAP) techniques are given to indicate the presence of targets in each data set.

Contents

List of Figures

List of Tables

1 Introduction

The Common Research Environment for Space-Time Adaptive Processing Technology (CREST) is a Defense Advanced Research Projects Agency (DARPA) sponsored effort under the Advanced Signal Processing (ASP) program (formerly the Mountaintop program) [9] to make available recorded radar data, high performance computing facilities, and signal processing tools to Space-Time Adaptive Processing (STAP) researchers. More information about the CREST environment can be accessed via the World Wide Web (WWW) CREST homepage, wwwcrest.mhpcc.edu.

In support of the CREST program the Air Force Rome Laboratory had been tasked to organize a challenge, the CREST Challenge, for the radar signal processing community. Presented with a number of simulated airborne phased array data sets, the researcher was challenged to resolve all target information. The objective of the challenge was not only to spark competition among researchers, but also to familiarize the radar signal processing community with the CREST assets.

There were four airborne multi-channel surveillance radar type data sets in the challenge; the first three consist of a single coherent processing interval (CPI) while the fourth contains multiple CPIs. Each data set was created with the Air Force Rome Laboratory Space-Time Adaptive Processing Algorithm Development Tool (RLSTAP/ADT). This tool is being developed as a user-friendly software package to aid researchers in generating and evaluating multi-channel surveillance radar data and STAP algorithms. Data and documentation for the challenge are accessible through the WWW via the CREST home page. The data sets are available in RLSTAP data format and MATLAB data format.

The purpose of this report is to document the generation and the properties of the CREST Challenge data sets. Understanding this report requires a basic understanding of the RLSTAP tool which was used for all data generation and signal processing results. Section 2 provides a basic overview of RLSTAP/ADT, data generation using

RLSTAP/ADT, and the CREST Challenge Radar. Section 3 describes the processing algorithms used in evaluating the data: conventional processing, factored time-space processing, adaptive displaced phase center array processing and joint domain processing. Section 4 describes the first data set of the challenge and will show some simple analysis results with conventional and STAP algorithms. The second data set, unlike the first where homogeneous clutter was used, uses geographical site specific information from the Delmar, Maryland area to generate clutter returns. The clutter type and signal scenario for this example will be described in Section 5 along with its analysis. Section 6 describes and analyzes the third data set, where clutter returns are derived from the Olympia, Washington area. Section 7 describes the fourth data set. The fourth data set actually consists of ten separate data sets, each being a consecutive coherent processing interval (CPI) in an airborne surveillance scenario. These data sets contain clutter returns from the Salt Lake City, Utah area. This last data set was generated as a near real-life situation that could occur in a surveillance situation. Conclusions are discussed in Section 8.

It must be emphasized that the purpose of this report is not to give an algorithm performance comparison among several data sets. The objective of this report is to document the characteristics of each CREST Challenge data sets. Any analysis is to verify the presence of targets or show the severity of the interference environment.

2 RLSTAP, Data Generation, and the CREST Challenge Radar

This section explains some of the fundamental characteristics of RLSTAP and its use in the generation of multi-channel radar data. For the CREST Challenge it is assumed that the surveillance radar is a multi-channel, square, phased array mounted on the side of an aircraft. The radar is monostatic and operates in a pulse-Doppler mode. The radar parameters are listed at the end of this section.

2.1 RLSTAP

RLSTAP/ADT is a user-friendly state-of-the-art software tool developed to help radar signal processing researchers analyze measured data, simulate airborne multi-channel radar data, develop and evaluate advanced signal processing algorithms, and assess system performance of advanced signal processing technologies [6]. The tool also provides a number of built-in diagnostic tools, including performance metrics, visualization aids, and a mathematics toolbox. RLSTAP is being developed by the Air Force Rome Laboratory (AFRL) under the DARPA ASP program to address next generation surveillance requirements [8].

RLSTAP uses the Khoros Software Development Environment which provides an easy to use graphical user interface (GUI). With the aid of a three button mouse one can quickly browse various processing options and create desired data simulation and signal processing routines. RLSTAP was used for both these purposes to support the CREST Challenge. A specific example data simulation using the GUI will be given in the next section. More information about the tool can be found on the CREST homepage.

2.2 Data Generation

For the CREST Challenge, all data generation was performed using RLSTAP. Figure 1 displays a typical RLSTAP data generation *lineup* in the Cantata work environment of Khoros. This particular lineup is referred to as the *physical model* (PM). A lineup is a
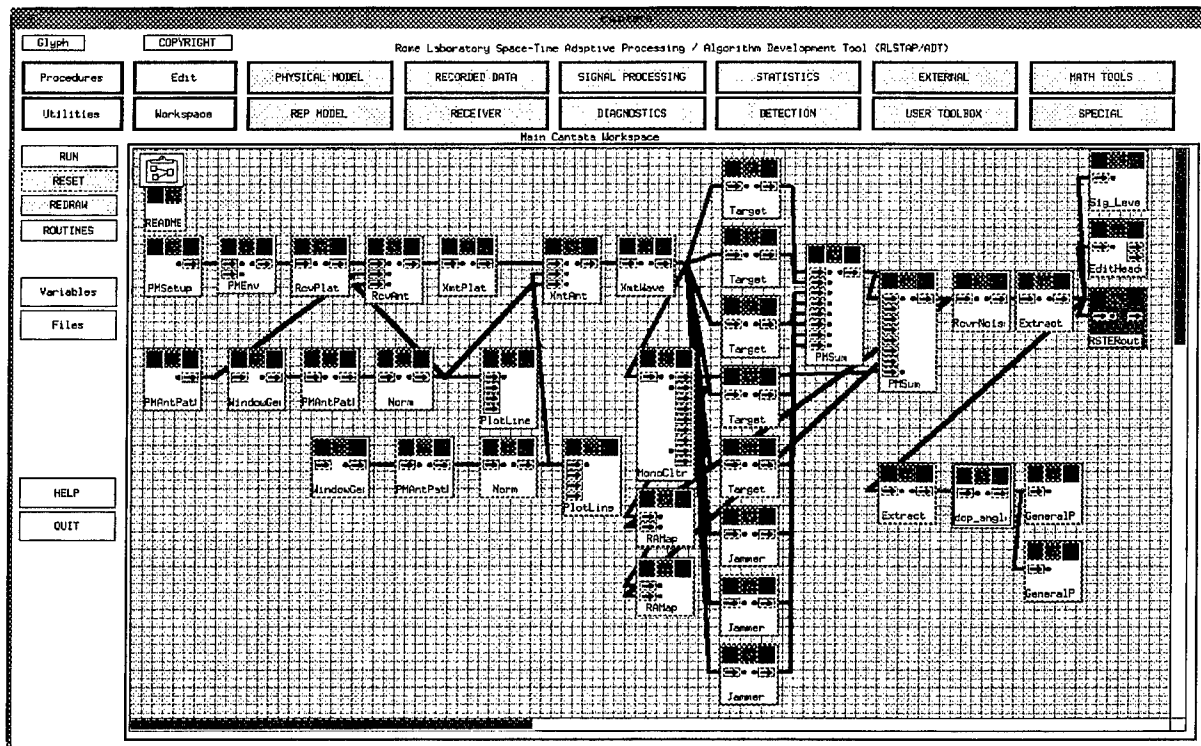
Fig. 1. RLSTAP Physical Model Lineup.

collection of *icons* or *glyphs*. Glyphs can be connected to perform a desired application where the logical flow of data follows the directions of the arrows in the glyphs.

The left most glyphs in Figure 1, labeled *PMSetup* and *PMEnv*, determine the operational range and azimuth of the radar and the clutter type. For preliminary studies and statistical analysis, a homogeneous clutter type may be chosen. For more detailed analysis of a particular geographic location clutter returns can be modeled using terrain height and terrain cover information available from the United States Geological Survey (USGS) database. Both homogeneous and site specific clutter were used for the challenge.

Proceeding along the processing chain, glyphs labeled *RcvPlat* and *RcvAnt* allow the user to specify the platform and antenna characteristics. Options for the platform consist of geographic location, altitude, heading, velocity, roll, pitch, yaw, phase center displacement, and data sampling frequency. Options for the antenna include azimuth and elevation patterns, number of elements in azimuth and elevation, mechanical boresight

12

direction, peak aperture gain, aperture efficiency, and aperture displacement. The glyphs following the receiver glyphs are used to specify similar information for the transmitter platform and antenna.

Following the receiver and transmitter glyphs is the transmit waveform glyph, *XmtWave*. Options for waveform type are pulse CW, LFM, and Barker. General user-specified parameters include peak transmit power, center frequency, pulse length, pulse repetition frequency, number of pulses and polarization. Additional parameters are transmit bandwidth, phase droop, phase jitter, phase offset, and waveform delay.

The most computationally expensive process of data generation is performed next in the glyph *MonoCltr* which generates the clutter returns given the desired model selected in *PMEnv*. Two models for clutter are available, homogeneous and site specific. The homogeneous clutter model applies a single clutter type across the entire surveillance volume. The site-specific clutter model simulates the clutter environment for a specified location using United States Geological Survey (USGS) terrain elevation and terrain cover data to determine such characteristics as visibility, grazing angle, and clutter type for each range-angle cell. Spatial and temporal clutter statistics are determined, or specified by the user, and are applied to each range-angle cell. Using the radar range equation and the information about each range-angle cell, RLSTAP computes a complex voltage for the clutter for each cell and stores that voltage in a *data cube* with dimensions or range, pulse, and element [6]. Also available from the *MonoCltr* glyph are clutter maps indicating terrain cover, terrain height, grazing angle, backscatter coefficient, backscatter, line of sight, clutter intensity, and Doppler. All maps are in range-angle polar form and have options such as overlaying range and angle grids and a scene plan indicating the location of targets and jammers relative to the platform. Examples of such maps is given later in this report.

Target information is added to the simulation with the *Target* glyph. The target glyph produces the radar returns given a point target with certain parameters. Target parameters such as range and azimuth from the platform, altitude, heading, speed, and

radar cross section may be specified. The Swerling RCS model may also be specified. For the CREST Challenge all targets were modeled as Swerling case 0.

Three types of jammer waveforms are available in RLSTAP, swept frequency, tone, and barrage noise. The latter type was used for all jammers in the challenge. Other jammer parameters that are specified by the user are range and azimuth from the platform, power, transmit frequency, bandwidth, period, duty factor, and sweep rate.

The returns from the clutter, targets and jammers are summed together for each range cell, element, and pulse to yield a range-pulse-element data cube of complex, base band, uncompressed voltage samples. The data cube generated by the lineup given in Figure 1 consists of only one CPI. Receiver noise is then added to the data with the glyph *RcvrNoise*. At this point the data is in RLSTAP readable format. The data may be transformed to MATLAB format. For the challenge data was given in both RLSTAP and MATLAB formats.

As mentioned previously, the CREST Challenge consisted of four data sets. The first three data sets each contain a single CPI while the last data set, CREST4, contains 10 CPIs. CREST4 actually consists of 10 separate data files (both in RLSTAP and Matlab format) where each file contains one CPI worth of data. Section 7 describes how each CPI represents a look or dwell at a particular position on the ground. During the time between dwells positions of targets, jammers, and the radar platform change. Because RLSTAP is not configured to generate a multiple CPI data set which takes into account target and platform trajectories, the RLSTAP physical model lineup must be run 10 separate times where parameters are changed to account for the new position of the targets, jammers, and platform. RLSTAP offers a batch job option which allows the user to specify files containing trajectory parameters, such as latitude and longitude of the platform, azimuth and elevation pointing angles for the receiver and transmitter, and range, azimuth, and altitude of targets from CPI to CPI. Figure 2 displays the Cantata work space with the batch job glyph PhymodBatch and its parameter list, or control pane, displayed. The parameters specified in this glyph will override any previously

14
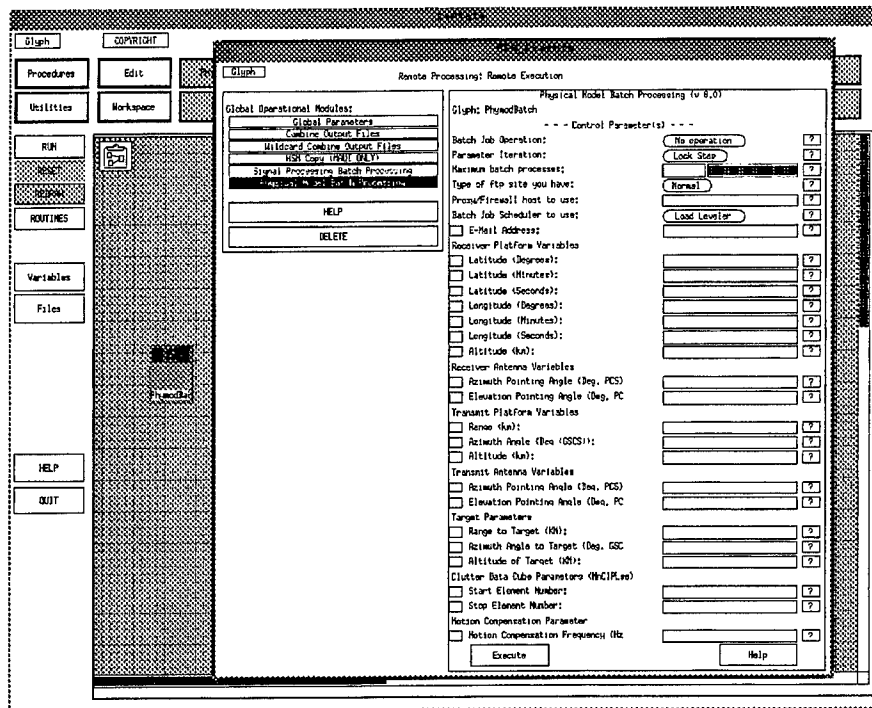
Fig. 2. Batch Job Processing in RLSTAP.

specified value in the appropriate glyphs in the physical model lineup. This glyph allows the user to run the batch job on the local machine or on a user specified remote machine.

2.3 CREST Challenge Radar

For the entire challenge a flying square phased array radar mounted on the side of an aircraft was simulated with the parameters as listed in Table 1. The radar operates in pulse-Doppler mode emitting M pulses in a CPI at a rate equal to the pulse repetition frequency (prf). The interval between pulses is referred to as the pulse repetition interval (pri) $T = \frac{1}{prf}$. The antenna is configured as having 20 elements (or channels) in azimuth. Each element in azimuth consists of 10 elements in elevation summed together with a 32.5 Dolph Chebyshev weighting pattern. On transmit the 20 azimuth elements are weighted with a rectangular weighting pattern. On receive each of the 20 azimuth elements is given a cosine pattern. Figure 3 and Figure 4 show the antenna gain patterns vs. elevation and azimuth angles respectively.

15

Table 1. CREST Challenge RADAR Parameters

Parameter	Value
tx frequency	450 MHz
wavelength (λ)	0.667 m
tx pulse width	$50\mu s$
tx bandwidth	.5 MHz
tx waveform	LFM
tx azimuth beamwidth	5°, rectangular weight
tx elevation beamwidth	13°, 32.5dB Dolph Cheb. weight
tx peak aperture gain	29.0 dB
prf	1.0 KHz
pulses	18
channels	20, in azimuth
element spac.	$.5\lambda$
sampling rate	1 MHz
rx azimuth beamwidth	each element - cosine pattern
rx elevation beamwidth	13°, 32.5dB Dolph Cheb. wgt
rx peak aperture gain	17.5 dB
rx aperture efficiency	1.0
insertion loss	1.5 dB
receiver gain	196.0 dB
rcvr pre-IF bandwidth	.5 MHz
rcvr noise figure	5.0 dB
antenna view temp	200°K
lossy component temp	290°K
rcvr reference temp	290°K

Other parameters including location of the platform (latitude, longitude and altitude), mechanical boresight direction, platform velocity, and platform heading were varied for each data set. For convenience platform heading and mechanical boresight azimuth will be given with respect to true North in the Geodetic Coordinate System (GCS) (clockwise, +), while direction of arrival (DOA) of target and jammer returns will be referenced to mechanical boresight. Mechanical boresight elevation will be given with respect to the platform horizontal (down looking, +).

16
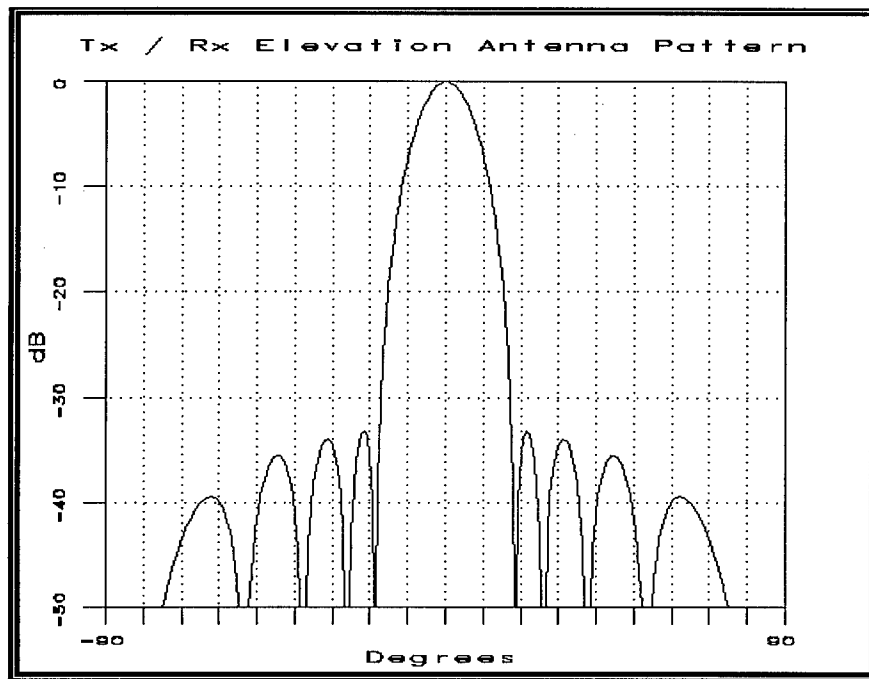
Fig. 3. Transmit and Receive Elevation Antenna Beam Pattern.
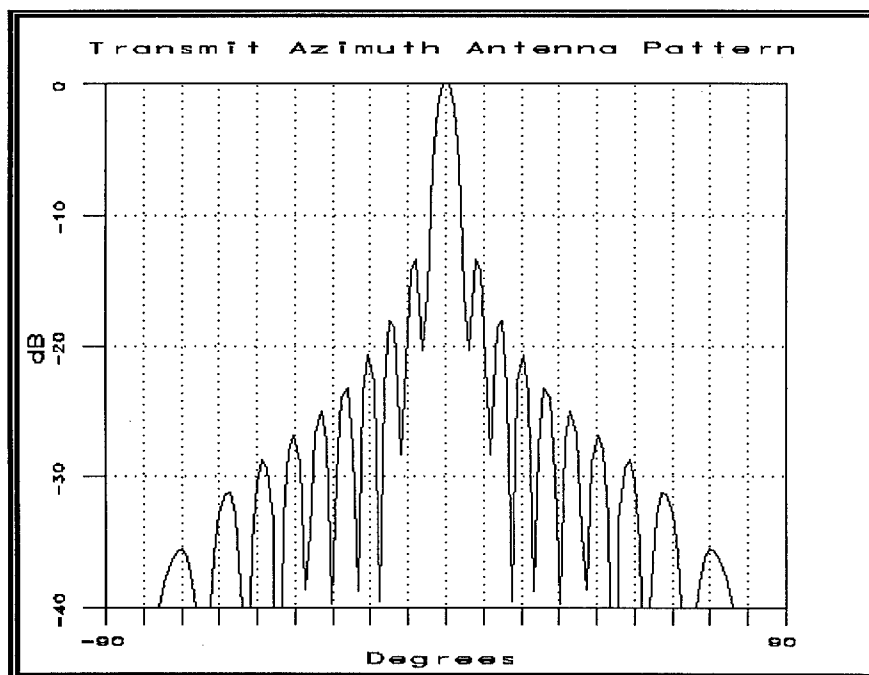
Fig. 4. Transmit Azimuth Antenna Beam Pattern.

17

3   Signal Processing Algorithms

In the following sections of this report, the properties for each CREST Challenge data set, such as clutter scene and target scenario, will be discussed. Given a surveillance radar data set from a phased array in range-pulse-element dimensions one may process the data set with a set of algorithms in order to determine target parameters such as azimuth angle, range, and Doppler frequency. For simplification of future discussions four algorithms used in this report are described in this section. References for the algorithm descriptions to be given include [1], [5], [8], and [10]. One conventional processing method and three STAP approaches will be described. Each algorithm is available as part of the signal processing capability in RLSTAP. Therefore, each algorithm will be described in the manner that RLSTAP implements it. The four algorithms discussed include conventional processing, factored time space processing, adaptive displaced phase center array processing , and joint domain processing. Also, a means for detection processing will be discussed.

Before proceeding to the algorithm descriptions some nomenclature is introduced. The surveillance radar under consideration consists of a multi-channel monostatic radar that emits a burst of M pulses and records the returns between successive pulses at each of the N azimuthal channels or elements. This burst of pulses represents a CPI. The time between pulses is the pri and the rate that the pulses are emitted is the prf (see Section 2.3). The L samples taken between pulse transmissions at the elements represent the returns from a given range extent, sometimes referred to as range cells. Let $\mathbf{x}_{m,l}$ be an $N \times 1$ vector of antenna element outputs at the *lth* range sample for the *mth* pulse, referred to as a *spatial* snapshot,

$$\mathbf{x}_{m,l} = [x_{1,m,l}\, x_{2,m,l} \,\cdots\, x_{N,m,l}]^{\mathbf{T}},\tag{1}$$

where $x_{n,m,l}$ is the basebanded complex voltage sample from the *nth* element, *mth* pulse, and *lth* rage cell. The returns received by the N elements due to the M transmitted pulses illuminating L range cells can be collected into a cube. The dimensions of the cube are
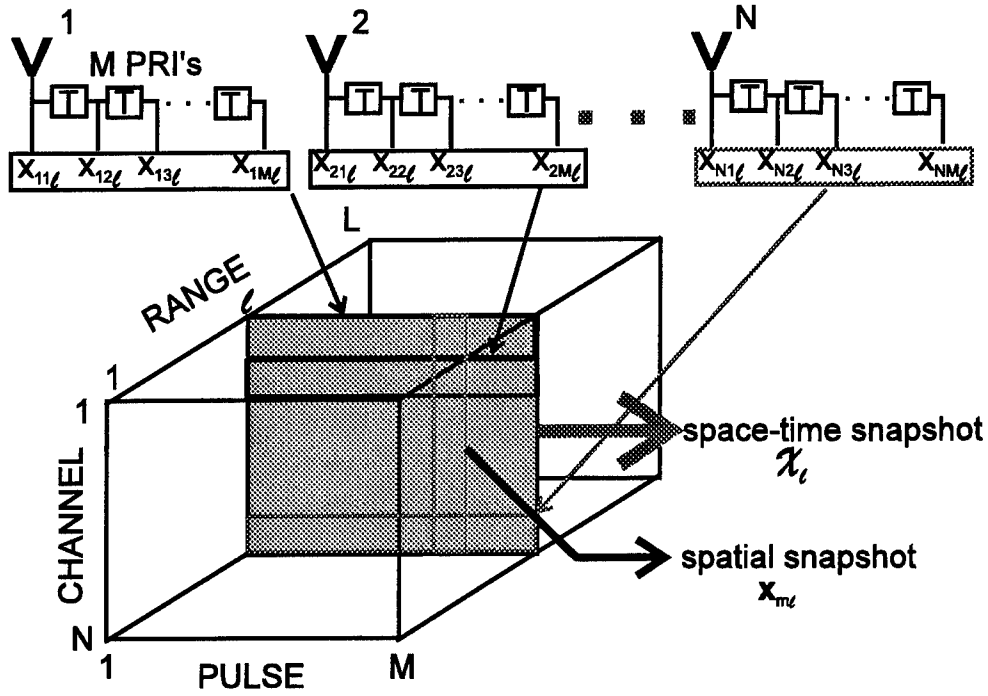
Fig. 5. The Radar Data Cube Structure.

range, element, and pulse as shown in Figure 5, or $L \times N \times M$. Here the returns for a given range cell from all the channels and all the pulses forms a *space-time* snapshot $\boldsymbol{\mathcal{X}}$ of dimension $N \times M$,

$$\boldsymbol{\mathcal{X}}_l = [\mathbf{x}_{1,l}\,\mathbf{x}_{2,l} \ldots \mathbf{x}_{M,l}]. \tag{2}$$

It is often convenient to write (2) as a $NM \times 1$ vector which is formed by stacking the columns of $\boldsymbol{\mathcal{X}}_l$,

$$\mathbf{x}_l = vec(\boldsymbol{\mathcal{X}}_l) = \begin{bmatrix} \mathbf{x}_{1,l} \\ \mathbf{x}_{2,l} \\ \vdots \\ \mathbf{x}_{M,l} \end{bmatrix}. \tag{3}$$

Equation 3 is also referred to as the *space-time* snapshot as is $\boldsymbol{\mathcal{X}}_l$, but in vector form.

There are two designations often used to refer to the data in the cube shown in Figure 5. There is primary data (or snapshots) and secondary data (or snapshots). The primary data are the snapshots (either spatial snapshots, $\mathbf{x}_{m,l}$, or a space-time snapshots, $\mathbf{x}_l$), or range cells, where a target signal may be present as well as interference. The particular

19

range cell under consideration in the primary data for containing a target is often referred to as a test cell. A region about the test cell is often designated as a guard region or guard cells and is part of the primary data. Data that contains interference only is termed secondary data. The interference in the secondary data is assumed to be independent and identically distributed to the interference in the primary data. Therefore, secondary data is used to adaptively cancel interference only in the primary data. Secondary data is often termed training data as it is the data used in training an adaptive weight vector. The method of selecting secondary data is crucial to the signal to noise ratio (SNR) performance of an algorithm and is a topic unto itself [3] [4].

Typically an algorithm will train an adaptive weight vector using secondary data and apply the weights to the primary data only. Another test cell is chosen along with another set of training data and the process is repeated. Often times it is convenient to train only once using one set of training data and apply the resulting weight vector to the entire (or portion of) data cube. This method is termed *freeze training*.

3.1 Conventional Processing

The simplest method of processing radar data is to use nonadaptive techniques. The advantages of such a method is that it is not as computationally expensive as its adaptive counterpart. The drawback, however, is that it is prone to interference entering the main lobe or sidelobes of the non-adaptive weight pattern. Figure 6 shows a typical RLSTAP lineup for conventional processing. As mentioned in Secton 2.2 data flow through the glyphs is from left to right.

The $L \times N \times M$ data cube is first pulse compressed with an appropriate matched filter. This operation improves not only SNR of the target but range resolution as well. The match filter waveform may be weighted beforehand, as indicated by the WindowGen glyph, in order to reduce range sidelobes.

Motion compensation is used next in the conventional processing chain to shift the frequency of the main beam clutter to DC if needed. Motion compensation is often

needed to compensate for misalignment between the heading vector of the aircraft and the pointing direction of mechanical boresight which, if not perpendicular to each other, induces a phase shift in time. Motion compensation removes this phase shift by applying a *conjugate* time phase shift to every element in the complex data cube.

Following motion compensation is a moving target indicator (MTI) which is used to perform standard main beam clutter suppression on the data cube using a fixed weight delay line canceler (DLC). Filtering is done in the time domain along the pulse dimension using a q tap DLC where $q = 2$ or 3. It should be noted that the number of pulses M in a data cube will be reduced by $q - 1$ after q pulse MTI processing.

The next operation in the processing chain is Doppler subbanding. This module in RLSTAP performs standard radar Doppler filtering on the input complex voltage data cube. Filtering is accomplished with a weighted DFT applied across the pulse dimension or rows of (2) to produce a transformed matrix,

$$\widetilde{\boldsymbol{\mathcal{X}}}_l = [\tilde{\mathbf{x}}_{1,l}, \tilde{\mathbf{x}}_{2,l}, \ldots, \tilde{\mathbf{x}}_{M,l}]. \tag{4}$$

Here $\tilde{\mathbf{x}}_{m,l}$ is a $N \times 1$ spatial snapshot obtained by collecting the terms of the *mth* Doppler filter for all the elements at the *lth* range gate. The weighting is used to reduce Doppler sidelobes. The filtering is done over all l range cells in the data cube and converts the $L \times N \times M$ range-element-pulse data cube to a $L \times N \times M$ range-element-Doppler data cube.

Following Doppler processing non-adaptive beamforming is performed. This is determined by the ConvRule (Conventional Rules) glyph which supplies information to the rest of the lineup that non-adaptive processing will be performed. Non-adaptive beamforming is performed by linearly combining the N element returns in each Doppler cell (or filter) for each range cell thereby converting the $L \times N \times M$ range-element-Doppler data cube into a $L \times M$ range-Doppler matrix of outputs. This is accomplished by taking the inner product of an $N \times 1$ vector s with the spatial snapshot $\tilde{\mathbf{x}}_{m,l}$,

$$y_{m,l} = \mathbf{s}^{\mathbf{H}} \tilde{\mathbf{x}}_{m,l}. \tag{5}$$

21
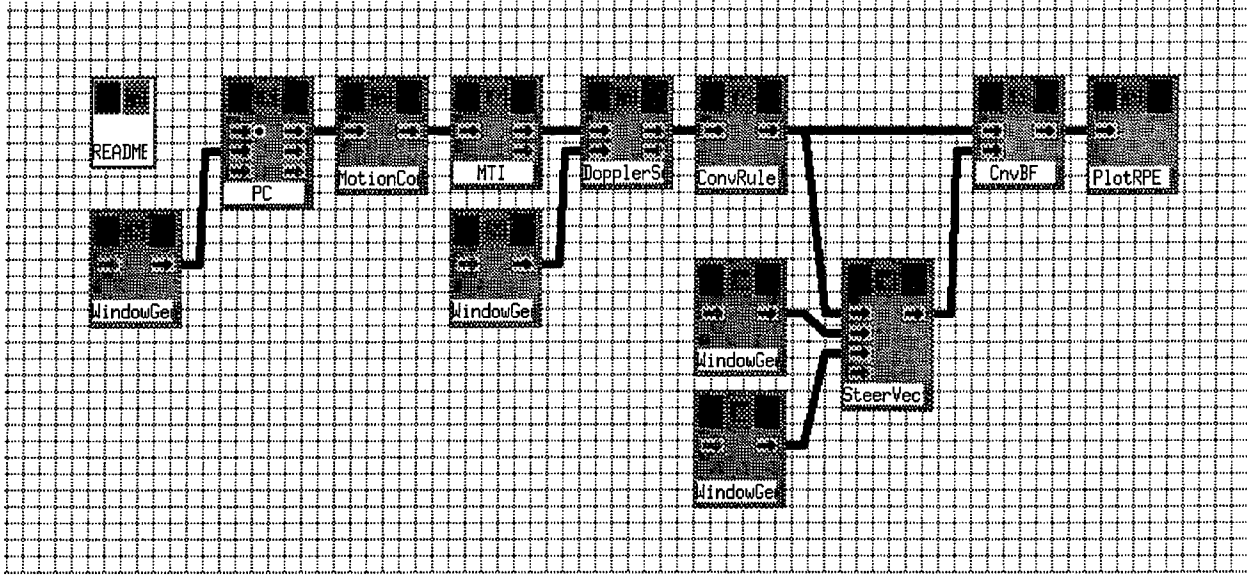
Fig. 6. Conventional Radar Signal Processing Lineup in RLSTAP.

Here $\mathbf{H}$ denotes the complex conjugate transpose and $y_{m,l}$ is the scalar output for the mth pulse and lth range cell. The power of $y_{m,l}$ can then be compared to a threshold in order to determine if a target is present in the mth Doppler filter at the lth range gate. The vector $\mathbf{s}$ is referred to as the spatial steering vector defined as,

$$
\mathbf{s} = \begin{bmatrix} w_{s1}1 \\ w_{s2}e^{j2\pi\psi} \\ \vdots \\ w_{sN}e^{j(N-1)2\pi\psi} \end{bmatrix},
\tag{6}
$$

where the *spatial frequency* $\psi = \frac{d}{\lambda}\cos\theta\sin\phi$. The angles θ and ϕ represent the look direction elevation and azimuth angles respectively measured relative to the array normal. The scalars $w_{s1} \ldots w_{sN}$ represent some weighting function.

Conventional processing can be performed in a number of ways. The method described above is just one example. The pulse compression, beamforming, and Doppler processing operations can be swapped in various combinations because they are linear operations.

22

3.2 Joint Domain Processing

Full space-time processing, sometimes referred to as Joint Domain (JD) processing, applies adaptive weights spatially and temporally. In other words adaptive weights are applied to all channels and pulses. This is an effective method for mitigating airborne radar clutter which is spread across angle and Doppler. At the same time, JD processing must mitigate jamming signals such as white noise barrage jamming which is discrete in angle and white in Doppler.

The JD algorithm determines an $NM \times 1$ weight vector $\mathbf{w_{jd}}$ which when applied to a to a test cell $\mathbf{x}_l$ via the inner product,

$$y_l = \mathbf{w_{jd}^H} \mathbf{x}_l, \tag{7}$$

maximizes the signal to interference plus noise ratio (SINR) [7]. The optimal weight vector $\mathbf{w_{jd}}$ for the full dimension space-time problem is defined by the Wiener-Hopf equation,

$$\mathbf{w_{jd}} = \mathbf{R_{jd}^{-1}} \mathbf{v}, \tag{8}$$

where $\mathbf{v}$ is a $NM \times 1$ target space-time steering vector and $\mathbf{R_{jd}}$ is an estimate of the true interference covariance matrix for the cell under test and is of dimension $NM \times NM$.

Interference in the test cell is estimated using training data snapshots as defined in (3). Typically the training data come from neighboring range cells about the test cell with the exception of a few guard cells. This makes the assumption that if a test cell lies within a forest cover type that neighboring test cells will also lie in forest cover type and provide similar statistics to those of the cell under test. This scenario obviously breaks down when the cell under test lies between two different cover types, i.e., mountains and water, where the clutter statistics may be drastically different from one cover type to the next. As a rule of thumb, a maximum likelihood estimate of the interference requires at least $2K$ independent and identically distributed (iid) snapshots [7]. Here K is the number of required degrees of freedom (DOF) for a given algorithm. The JD algorithm

requires $K = NM$ DOF. The estimate of $\mathbf{R_{jd}}$ is given by,

$$\mathbf{R_{jd}} = \frac{1}{2K} \sum_{2K\,snapshots} \mathbf{x}_k \mathbf{x}_k^{\mathrm{H}} \tag{9}$$

It should be noted that if $\mathbf{R_{jd}}$ is the true interference covariance matrix then $\mathbf{w_{jd}}$ is optimal and the algorithm is often referred to as Joint Domain Optimum (JDO). The acronym JDO is often used in place of JD with the understanding that an estimate of $\mathbf{R_{jd}}$ was used.

The target space-time steering vector $\mathbf{v}$ in (8) is defined by the kronecker product of the temporal steering vector t and the spatial steering vector s,

$$\mathbf{v} = \mathbf{t} \otimes \mathbf{s}, \tag{10}$$

where $\mathbf{t}$ is defined by,

$$\mathbf{t} = \begin{bmatrix} w_{t1}1 \\ w_{t2}e^{j2\pi\omega} \\ \vdots \\ w_{tM}e^{j(M-1)2\pi\omega} \end{bmatrix}. \tag{11}$$

Here the *normalized Doppler frequency* $\omega = \frac{f_d}{prf}$ where f_d is the target Doppler frequency and prf is the pulse repetition frequency. The scalars $w_{t1} \dots w_{tM}$ represent some weighting function.

Figure 7 shows a typical RLSTAP JD processing lineup. Preprocessing of the radar cube is typically performed by applying pulse compression as described in Section 3.1. The glyph JDORule sets the training data selection (secondary data) and range cells to be beamformed (primary data) as in (7).

The glyphs Covar, DiagLoad, and InvCovar perform covariance estimation, diagonal loading and inversion of the covariance matrix respectively. The covariance matrix is computed as in (9) using the rules from JDORule for secondary data selection. Diagonal loading adds a small noise term to the main diagonal of the covariance matrix to prevent ill-conditioning during the inversion process.

The glyph SteerVec provides M $NM \times 1$ space-time steering vectors $\mathbf{v}$ as defined in (10) steered in both angle and Doppler. The spatial look direction angles are specified in this
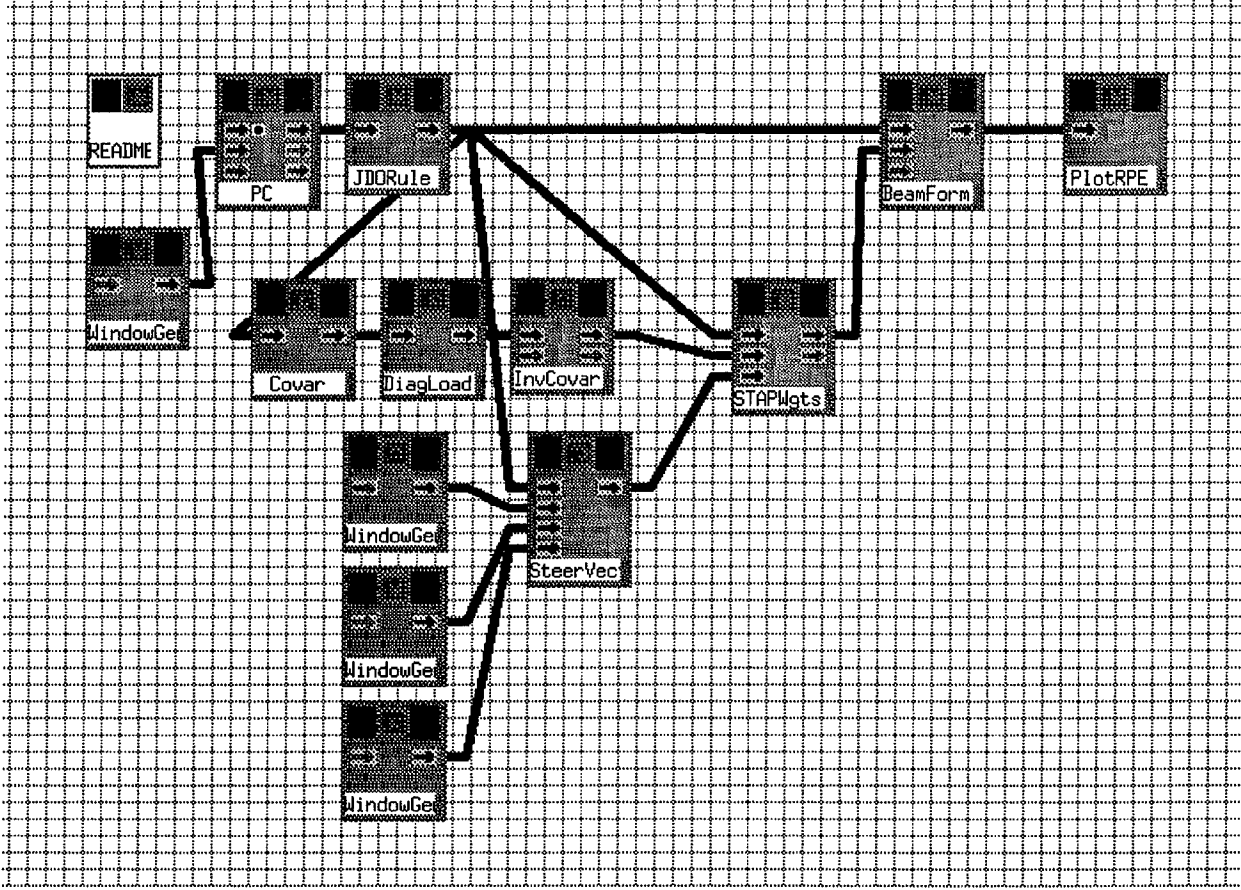
Fig. 7. Joint Domain Optimal Radar Signal Processing Lineup.

glyph and are the same for all M vectors. The normalized Doppler frequency, $\omega = \frac{f_d}{prf}$, in (10) is pre-specified by the center frequency of each of the M Doppler filters which span the PRF interval, hence making M distinct space-time steering vectors. The spatial weights $w_{s1} \ldots w_{sN}$ and temporal weights $w_{t1} \ldots w_{tM}$ are defined in the WindowGen glyphs.

The STAPWgts glyph determines the appropriate $NM \times 1$ weight vectors for each of the M Doppler filters as defined in (8). Beamforming is then done with the BeamForm glyph where the M weight vectors are applied to the primary range cells defined in JDORule in the appropriate Doppler filter as in (7). Typically freeze training is used and the adaptive weight vector is applied to all range snapshots (both primary and secondary

25
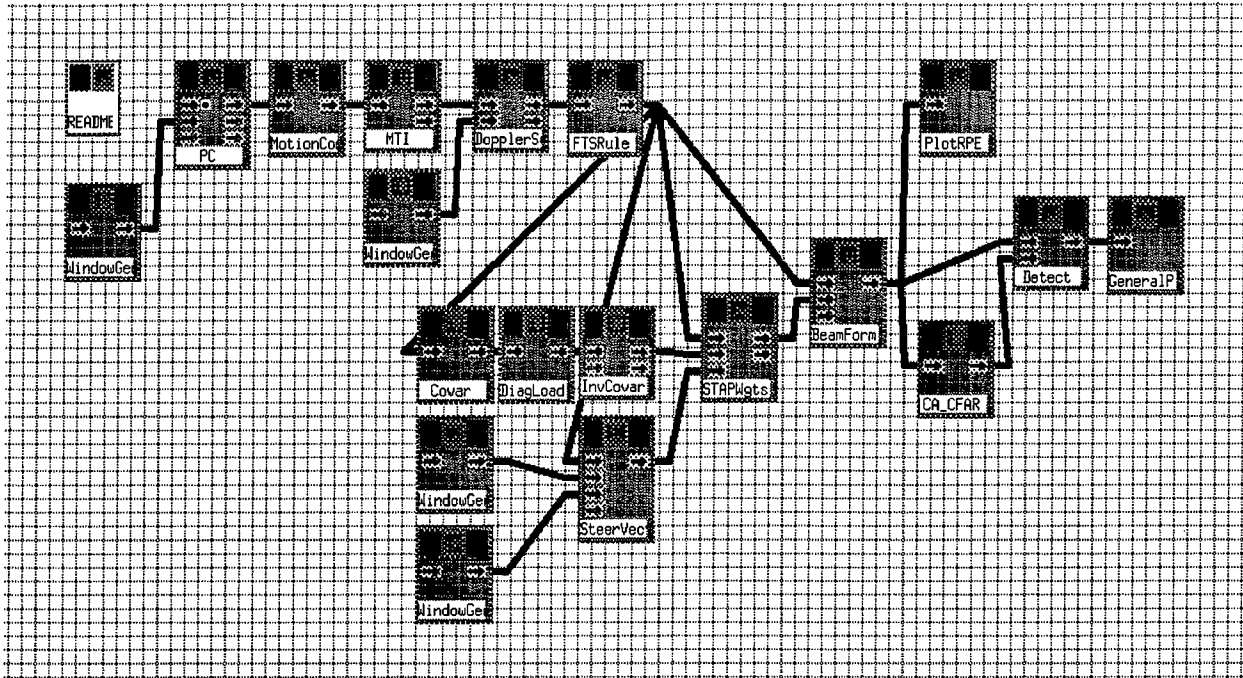
Fig. 8. Factored Time Space Radar Signal Processing Lineup.

data) and results in a $L \times M$ range-Doppler matrix of output values whose power can be compared to a threshold to determine if a target is present.

3.3 Factored Time Space Processing

Because of the large computational cost of determining $\mathbf{R_{jd}}$ and $\mathbf{R_{jd}^{-1}}$, it is advantageous to consider partially adaptive STAP techniques. One such algorithm is the Factored Time Space (FTS) algorithm, also referred to as a post-Doppler adaptive beamformer. The objective of this algorithm is to perform conventional Doppler processing on the radar data cube first, followed by adaptive beamforming in each of the M Doppler filters. The Doppler filtering suppresses mainlobe clutter nonadaptively and localizes competing sidelobe clutter in angle whereby spatial adaptive beamforming is applied to place nulls in the direction of sidelobe clutter and jammers [10]. In a strict sense this is not STAP processing because only spatial adaptive weights are found.

The FTS algorithm output is the inner product of an $N \times 1$ adaptive weight vector

26

$\mathbf{w}_{\mathbf{fts},m}$ and the transformed spatial data snapshot from (4) corresponding to the mth Doppler filter and lth range gate,

$$y_{m,l} = \mathbf{w}_{\mathbf{fts},m}^{\mathbf{H}} \tilde{\mathbf{x}}_{m,l}. \tag{12}$$

Because adaptive beamforming is performed in each Doppler filter, FTS processing requires M, $N \times 1$ adaptive spatial weight vectors given by,

$$\mathbf{w}_{\mathbf{fts},m} = \mathbf{R}_{\mathbf{fts},m}^{-1} \mathbf{s}. \tag{13}$$

Here, $\mathbf{R}_{\mathbf{fts},m}^{-1}$ is an estimate of the interference covariance matrix for the cell under test in the mth Doppler filter and is of dimension $N \times N$. The $N \times 1$ vector s is the spatial steering vector given in (6). The covariance matrix is found by,

$$\mathbf{R}_{fts,m} = \frac{1}{2K} \sum_{2K\,snapshots} \tilde{\mathbf{x}}_{m,k} \tilde{\mathbf{x}}_{m,k}^{\mathbf{H}}. \tag{14}$$

As with the JD algorithm, or any algorithm requiring a covariance estimate, the rule of thumb is to have at least $2K$ iid snapshots or training data snapshots. Here $K = N$ is the required DOF for the FTS algorithm.

Figure 8 shows a typical RLSTAP FTS lineup. The FTS filtering is preceded by pulse compression, motion compensation, and MTI filtering as described in Section 3.1. The FTS portion of the lineup begins with conventional Doppler processing on the radar data cube, as described in Section 3.1, with the glyph DopplerSub. This results in an $L \times N \times M$ range-element-Doppler data cube where the lth data snapshot is given in (4).

The FTSRule glyph specifies for the rest of the lineup the secondary (training) and primary data to use for covariance estimation and beamforming, respectively. The glyphs Covar, DiagLoad, and InvCovar use this information to estimate the interference covariance matrix in each Doppler filter as in (14).

The glyph STAPWgts uses the M covariance estimates to generate M ($N \times 1$) spatial adaptive weight vectors as in (13). The BeamForm glyph applies the M weight vectors to the primary data in the respective Doppler filters as in (12). Typically the adaptive

weight vectors are applied to all the range snapshots (both primary and secondary data), i.e. freeze training. This produces an $L \times M$ range-Doppler matrix of output values whose power can be compared to a threshold to determine if a target is present. Figure 8 includes three glyphs, CA_CFAR, Detect, and GeneralIP which generate a detection map output. This process is discussed in Section 3.5.

3.4 Adaptive Displaced Phase Center Array Processing

Another common partially adaptive STAP algorithm is the Adaptive Displaced Phase Center Array (ADPCA) processing algorithm. ADPCA processing is a pre-Doppler partially adaptive STAP beamformer. This algorithm consists of full spatial adaptivity and partial temporal adaptivity because it only uses P pulses at a time. Typically P is 2 or 3 and will be referred to here as the pulse window. A binomial weight is applied across the pulses to steer the peak of the Doppler response to the center of the PRF interval and place a null at DC [8]. If the main beam clutter has been shifted to DC, with motion compensation for example, this pulse differencing scheme will remove the clutter. Integration gain can be obtained by Doppler processing after ADPCA filtering as discussed in Section 3.1.

An output for the pth pulse window and lth range cell for the ADPCA algorithm is defined as,

$$y_l^p = (\mathbf{w}_{\mathbf{adpca}}^p)^{\mathbf{H}} \hat{\mathbf{x}}_l^p \tag{15}$$

where $1 \leq p \leq M - P + 1$. The $NP \times 1$ vector $\hat{\mathbf{x}}_l^p$ is a space-time snapshot vector similar to (3). Define a new space-time snapshot,

$$\widehat{\boldsymbol{\mathcal{X}}}_l^p = [\mathbf{x}_{p,l} \, \mathbf{x}_{p+1,l} \, \ldots \, \mathbf{x}_{p+P-1,l}], \tag{16}$$

where $\mathbf{x}_{p,l}$ is a $N \times 1$ spatial snapshot for the pth pulse and lth range cell. Stacking the

28

columns of $\widehat{\boldsymbol{\mathcal{X}}}_l^p$ yields a convenient form

$$\hat{\mathbf{x}}_l^p = vec(\widehat{\boldsymbol{\mathcal{X}}}_l^p) = \begin{bmatrix} \mathbf{x}_{p,l} \\ \mathbf{x}_{p+1,l} \\ \vdots \\ \mathbf{x}_{p+P-1,l} \end{bmatrix}. \tag{17}$$

Following the form of the full JD weight vector given in (8), the $NP \times 1$ ADPCA adaptive weight vector is given as,

$$\mathbf{w}_{\mathbf{adpca}}^p = (\mathbf{R}_{\mathbf{adpca}}^p)^{-1}\hat{\mathbf{v}}, \tag{18}$$

where $\mathbf{R}_{\mathbf{adpca}}^p$ is an estimate of the true interference covariance matrix for the cell under test in the pth pulse window and is of dimension $NP \times NP$. The vector $\hat{\mathbf{v}}$ is a $NP \times 1$ space-time steering vector.

The estimate of $\mathbf{R}_{\mathbf{adpca}}^p$ is given by,

$$\mathbf{R}_{adpca}^p = \frac{1}{2K} \sum_{k=2K \; snapshots} \hat{\mathbf{x}}_k^p (\hat{\mathbf{x}}_k^p)^{\mathbf{H}} \tag{19}$$

Here K is the number of required degrees of freedom (DOF) for a given algorithm. The ADPCA algorithm requires $K = NP$ DOF.

The steering vector $\hat{\mathbf{v}}$ is given by the kronecker product,

$$\hat{\mathbf{v}} = \hat{\mathbf{t}} \otimes \mathbf{s}, \tag{20}$$

where $\hat{\mathbf{t}}$ is $P \times 1$ vector defined by a binomial weight set,

$$\hat{\mathbf{t}} = \begin{bmatrix} b_1 \\ b_2 \\ \vdots \\ b_P \end{bmatrix}. \tag{21}$$

Because P is either 2 or 3, the scalars $[b_1 \ldots b_P]$ take on the values $[1, -1]_{P=2}$ or $[1, -2, 1]_{P=3}$.

Figure 9 displays the lineup for ADPCA processing in RLSTAP. Typical pre-processing of the data cube includes pulse compression and motion compensation. Motion compensation is necessary in order to account for any frequency shift of the main beam clutter

29
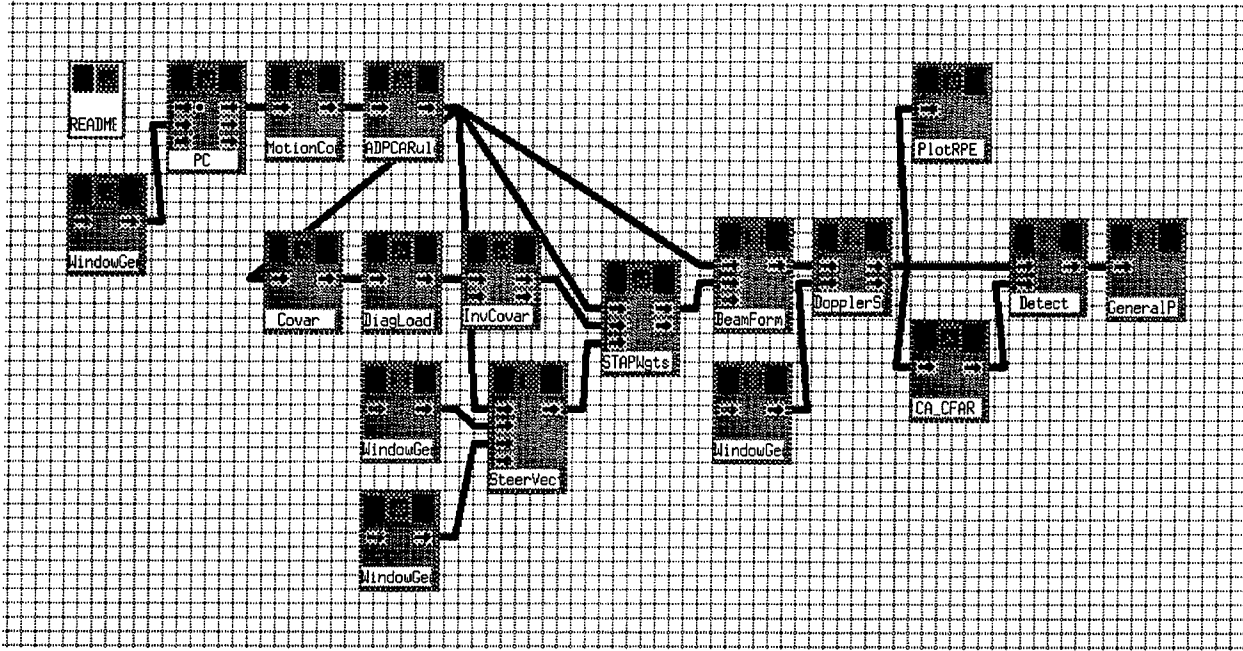
Fig. 9. **Adaptive Displaced Phase Center Array Radar Signal Processing Lineup.**

from DC. This is essential for the pulse differencing approach that the ADPCA algorithm employs to cancel main beam clutter. The ADPCARule glyph specifies for the rest of the lineup the secondary and primary data to use for covariance estimation and beamforming respectively. ADPCARule also allows the user to specify the value of P, either 2 or 3 pulse ADPCA.

The Covar glyph estimates the covariance matrix using the rules in ADPCARule. In RLSTAP only the $p = 1$ covariance estimate is found as defined in (19). That is, only the data in the first P pulses of the radar data cube are used to estimate one covariance estimate and in turn only one adaptive weight vector is found and used on the entire CPI. RLSTAP makes the assumption that little or no changes in the interference characteristics will occur within a CPI [8]. For example, Covar will calculate $\mathbf{R}^1_{\mathbf{adpca}} = \frac{1}{2K} \sum_{k=2K} \hat{\mathbf{x}}^1_k (\hat{\mathbf{x}}^1_k)^{\mathbf{H}}$. This estimate is then used by STAPWgts, along with the input from SteerVec which determines $\hat{\mathbf{v}}$, to find $\mathbf{w}^1_{adpca} = (\mathbf{R}^1_{\mathbf{adpca}})^{-1}\hat{\mathbf{v}}$. The user can specify the azimuth and elevation look directions used by $\hat{\mathbf{v}}$. BeamForm is then used to implement

30

(15). The filtered outputs for the lth range cell are calculated as $y_l^1 = (\mathbf{w}_{\mathbf{adpca}}^1)^{\mathbf{H}}\hat{\mathbf{x}}_l^1$, $y_l^2 = (\mathbf{w}_{\mathbf{adpca}}^1)^{\mathbf{H}}\hat{\mathbf{x}}_l^2, \ldots, y_l^{M-P+1} = (\mathbf{w}_{\mathbf{adpca}}^1)^{\mathbf{H}}\hat{\mathbf{x}}_l^{M-P+1}$.

The values of y_l^p, filtered output magnitudes for the lth range cell and pth pulse window, are collected into a $L \times (M - P + 1)$ matrix. It is assumed here that freeze training is employed and the adaptive weights are applied to both the primary and secondary data. This matrix of values is then sent to DopplerSub where conventional Doppler processing is employed and provides integration gain. The result is a $L \times (M - P + 1)$ range-Doppler matrix of outputs whos power can be compared to a threshold to determine if a target is present.

3.5 Detection Processing

Clutter, jamming, and thermal noise may still exceed target return levels after adaptive processing. In addition, false alarms may also appear. A threshold must be set to compare with the power of each range-Doppler cell (or range-angle cell) after adaptive filtering to determine the presence or absence of a target. The constant false alarm rate (CFAR) processor performs such a task by determining a threshold using local clutter statistics so that a constant false alarm rate is maintained for the entire range-Doppler map.

RLSTAP allows the user to partition the range-Doppler matrix, or map, about a test cell. The CFAR glyph, in Figures 8 and 9, takes the range-Doppler map as input and partitions it to determine a statistic for each test cell. The test cell refers to the range-Doppler cell in the map which is under test for the presence of a target. The statistic is then passed to a Detect glyph where a threshold is chosen for each test cell so as to maintain the CFAR specified by the user. The thresholds are then compared with the respective powers of each cell in the range-Doppler map in order to determine the presence or absence of a target [8].

RLSTAP provides four CFAR algorithms from which to choose. These include cell averaging (CA), greatest-of (GO), ordered statistics (OS), and trimmed mean (TM).

31

Each algorithm uses the partitioned data to determine a statistic for each cell under test. For the CREST challenge CA CFAR was chosen as the primary processor. Partitioning was done in each Doppler filter along the range dimension even though RLSTAP allows partitions in both range and Doppler. Given the number of data sets in the challenge, a rough method of choosing which range cells to keep in the partition for each test cell was used. On either side of each test cell an equal number of range cells was used, referred to here as the *CFAR window*, with no guard band in the statistic calculation. For CA CFAR, the mean of the cells in the CFAR window was the desired statistic.

The Detect glyph is used to estimate and apply a threshold value to the cell under test. The cell threshold is given as,

$$Cell\ Threshold\ =\ CFAR\ Statistic\ *\ Threshold\ Multiplier \tag{22}$$

As mentioned above, the CA CFAR Statistic is the average of the cells in the CFAR window. The threshold multiplier is either user specified as a fixed value, or determined in RLSTAP given the probability of false alarm (pfa) and a bias compensation factor C. In the case where the threshold multiplier T is not specified, RLSTAP calculates it as [8]

$$T = C\frac{4}{\pi}\ln(\frac{1}{pfa}). \tag{23}$$

Once T is found for each test cell, the cell threshold given in (22) is calculated and compared to the power of the respective range-Doppler cell. If the value for the test cell exceeds the threshold, a target is declared and is indicated on a range-Doppler detection map. Examples of detection maps are given later in this report when processing results of the CREST Challenge data sets are discussed.

4 Data Set 1 - CREST1

The first data set of the challenge, CREST1, was installed on the CREST homepage in mid-April 1996 along with all radar, target, jammer, and clutter environment parameters. CREST1 was to function as a warm-up case with easily detectable targets in a benign clutter environment. This data set was configured to familiarize novice RLSTAP users with the software tool's processing capabilities.

4.1 Overview

The simulated airborne platform was at an altitude of 20,000 feet heading due North with the radar mechanical boresight pointed due West and down 3°. Table 2 gives all the relevant platform information as well as clutter scene parameters. Recall that heading and mechanical boresight azimuth are given with respect to true North. Mechanical boresight elevation is given relative to platform horizontal.

The scenario was simulated with a homogeneous clutter environment with forest cover type. Power levels for thermal noise and the clutter to noise ratio are given in Table 3 as well as the parameters of each of the five targets and three jammers included in the scene. As mentioned in Section 2.2, various maps are available from the clutter generation process which help to visually describe the scene. Figure 10 displays an RLSTAP generated terrain cover map in polar format (range vs. angle) for CREST1. The cover types are either user specified for homogeneous clutter, or are derived from USGS data for site specific clutter examples. As can be seen for this example the entire area is of one type, forest, thus making the clutter returns homogeneous. Overlaid on top of the cover map is a scene plan indicating locations of targets and jammers. Each concentric ring on the map represents a 10 km increment where the center of the rings represents the location of the radar platform. Note that the operational range indicated on the cover map extends to 140 km which is within the unambiguous range for the CREST Challenge radar. The large arrow in the center of the range rings represents

33

Table 2. CREST1 Platform and Clutter Parameters

Parameter	Value
latitude	-
longitude	-
altitude	6.096 km
velocity	166.7 m/s
heading	0° (North)
mechanical boresight azimuth	270° (West)
mechanical boresight elevation	+3° (down)
recording start range	7 km
number of range samples	888
clutter scenario	homogeneous, forest
terrain spatial backscatter fluctuations	exponential
terrain temporal backscatter fluctuations	nonfluctuating
sea spatial backscatter fluctuations	-
sea temporal backscatter fluctuations	-
season	summer
sea state	-
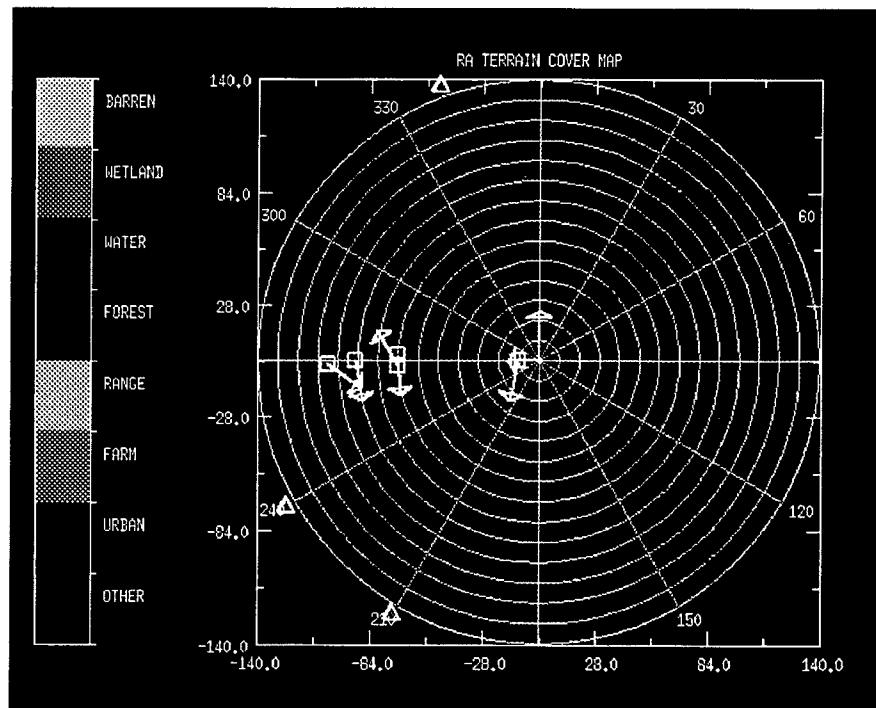
Fig. 10. Terrain Cover Map for CREST1.

Table 3. CREST1 Signal Scenario

Signal	Range,km (bin no.)	Az.	Doppler,Hz (bin no.)	SNR,dB
thermal noise	-	-	-	53.7
clutter to noise	-	-	-	68.8
target 1	10 (21)	4.04°	-100.8 (17)	12.66
target 2	70 (421)	−2.0°	-299.1 (14)	-6.51
target 3	70 (421)	2.50°	100.3 (3)	-1.76
target 4	91.4 (564)	0.00°	196.22 (5)	1.60
target 5	104.7 (652)	−1.0°	475.89 (10)	-0.86
jammer 1	145	70.0°	-	54.78
jammer 2	145	−30.0°	-	67.85
jammer 3	145	−60.0°	-	53.08

the platform heading while the mechanical boresight of the antenna is represented by the small arrow. Target locations in the scene are represented by small squares with the target heading represented by the small arrow emanating from the square. Jammer locations are identified by the small triangles. The specific location of each target in terms of range, angle, and Doppler is given in Table 3 as well as jammer locations. The SNR stated in the table, and for the entire report, refer to the signal return power at the output of the receiver with respect to receiver noise power on a per channel per pulse basis. All targets for CREST1 were positioned to lie inside the transmit main beam both in elevation and azimuth.

Figure 11 displays the clutter intensity for the scene in CREST1 in range vs. angle. Clutter intensity is the power measured at the receiver channels taking into account line of sight visibility, clutter backscatter, range, transmit power, antenna gain, and system losses [8]. The plot displays the average clutter power for the entire CPI. As can be seen in this particular case, the clutter returns are benign as one would expect from a homogeneous cover type.

Figure 12 shows the magnitude of the frequency spectrum in azimuth angle vs. Doppler for CREST1 at range cell 421. The plot indicates the three white noise barrage jammers which fill the entire Doppler spectrum at discrete angles. The *ridge*, extending diagonally
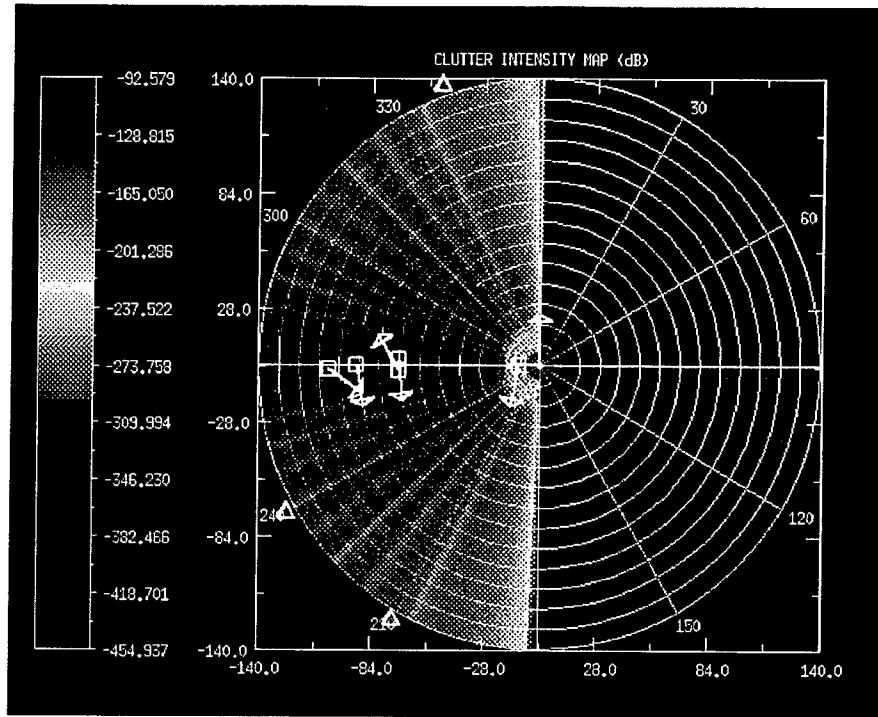
Fig. 11. Clutter Intensity Map for CREST1.

across the plot, represents the mainlobe and sidelobe clutter energy. The slope of this ridge is proportional to the velocity of the platform and inversely proportional to the prf of the radar. The slope of the ridge is defined as $\beta = \frac{4v}{\lambda(prf)}$ [10]. Here λ is the radar wavelength. For this example $\beta = 1$. For values of $\beta > 1$ the sidelobe clutter aliases in the Doppler dimension and the clutter returns become Doppler ambiguous. For values of $\beta \leq 1$ the clutter returns are unambiguous in Doppler. For the entire challenge platform and radar parameters were chosen such that $\beta \leq 1$. Also note from Figure 12 that targets 2 and 3 should appear in spectrum at range cell 421 but are not observable. Further processing gain is required in order to detect these two targets.

4.2 CREST1 Processing Results

Because of the relatively simple nature of the target and clutter scenario, detection of targets was not expected to be difficult. For this reason conventional processing, as

36
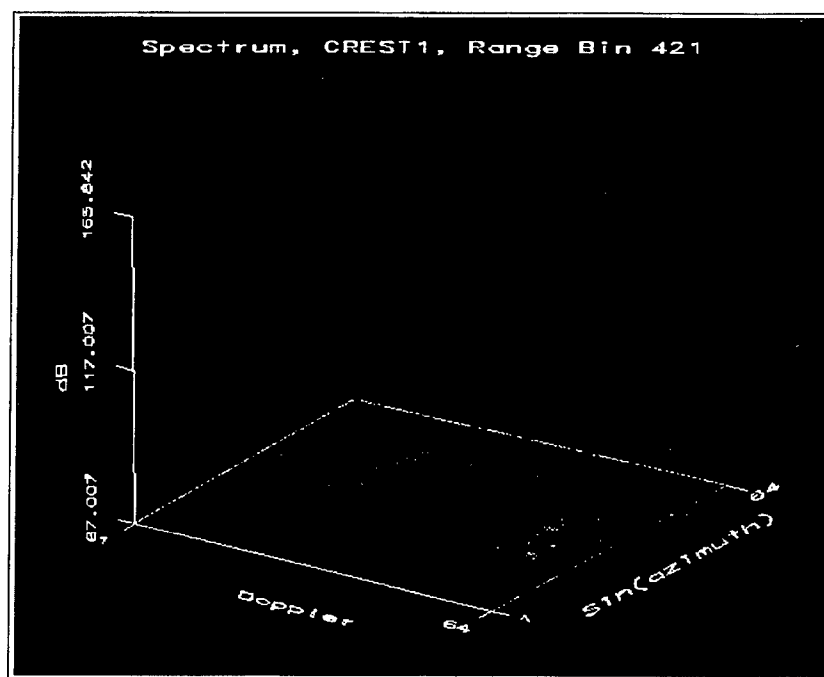
Fig. 12. Data Spectrum of CREST1, Range Cell 421.

Table 4. Conventional Beamforming, CREST1

Parameter	Description
pulse compression	LFM(50 μsec, 0.5 MHz), Hamming weight
motion compensation	none
MTI	3 pulse
Doppler filtering	Hamming weight
steering vector spatial az. weight	80 dB Chebyshev
steering vector spatial el. weight	rectangular
CFAR	none
pfa	none

described in Section 3.1, was applied to CREST1. Table 4 lists the parameters associated with the conventional beamforming lineup given in Figure 6. Note that the spatial steering vector was pointed in the same direction as the transmit beam which was pointed along the mechanical boresight. Figure 13 shows the power of the output after non-adaptive beamforming in a classic range-Doppler plot. Note that the range is given in

37
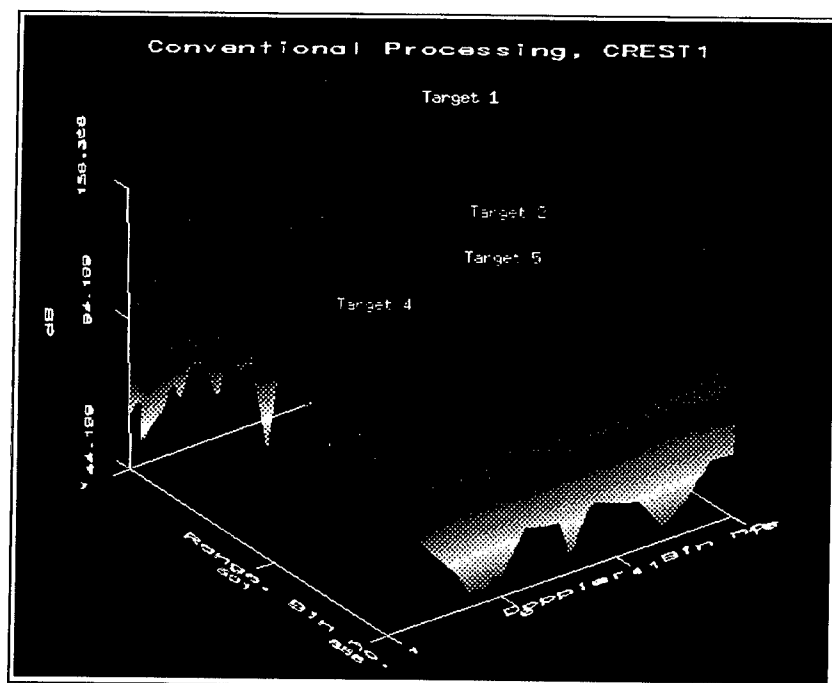
Fig. 13. Conventional Processing Applied to CREST1.

range bin (or cell) number and Doppler is given as Doppler bin number. All targets
are visually detectable except target 3 which is obscured by main beam clutter. The
main beam clutter primarily fills the first and last Doppler bins which represent the
frequencies near DC. Adaptive processing both temporally and spatially will be able to
retrieve target 3 from the clutter.

CREST1 was analyzed with a fully adaptive JD algorithm as described in Section 3.2.
Table 5 lists the parameters for JD processing of CREST1. For the CREST Challenge,
the number of pulses is $M = 18$ and the number of channels is $N = 20$. Therefore the JD
algorithm requires at least $2NM$, or 720 training samples. The training region for this
example slightly exceeds this number. Note that the spatial steering vector was pointed
in the same direction as the transmit beam which was pointed along the mechanical
boresight.

It is possible to detect the targets in CREST1 by simply applying the adaptive weights

38

Table 5. Joint Domain Processing, CREST1

Parameter	Description
pulse compression	LFM(50 μsec, 0.5 MHz), Hamming weight
training range cells (no.)	1 - 850
guard cells (no.)	396 - 446
diagonal loading (w/r peak)	-55 dB
steering vector spatial az. weight	Hamming
steering vector spatial el. weight	rectangular
steering vector temporal weight	30 dB Chebyshev
CFAR	none
pfa	none
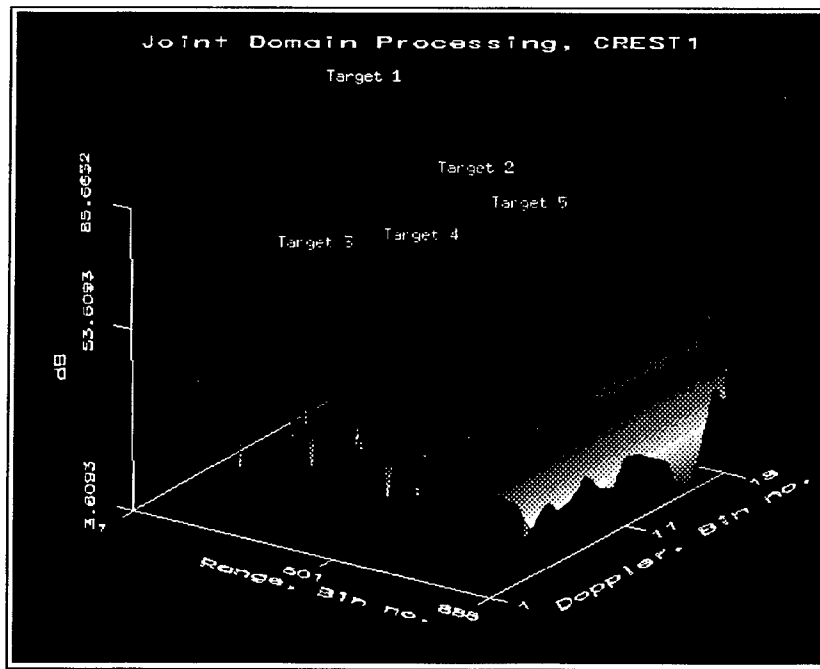
Fig. 14. Joint Domain Processing Applied to CREST1.

to the radar data cube and plotting the resulting output power on a range-Doppler map, see Figure 14. Clearly all targets are detectable including target 3. Other adaptive algorithms and training strategies have shown results similar to those in Figure 14 but are not given for the sake of brevity.

5 Data Set 2 - CREST2

The second data set of the challenge, CREST2, was installed on the CREST homepage in early June 1996. For this data set, and the remaining data sets in the challenge, target and jammer information were not provided to the challenger. It was up to the challenger to determine target range, angle (azimuth), and Doppler given only the radar parameters and the range-element-pulse data cube. Unlike CREST1 which used one cover type to provide homogeneous clutter returns, this data set utilizes RLSTAP's capability to generate clutter returns from site specific geographic areas. For this example the area near the Delmar Maryland was chosen.

5.1 Overview

The simulated airborne platform was at an altitude of 20,000 feet heading in a North-easterly direction. The radar mechanical boresight was perpendicular to the heading vector in azimuth and pointed in a North-westerly direction, off the port side of the aircraft. The mechanical boresight was pointed down 2.5° in elevation angle. The velocity of the platform was chosen such that the slope of the clutter ridge was $\beta = .5$. All platform specific parameters are given in Table 6 as well as information about the clutter scenario.

The geographic scene for CREST2 was centered about the Delmar Maryland area. RLSTAP used site specific data from the USGS data base to build maps for line of sight visibility, terrain cover, terrain height, and backscatter. The Delmar area offers many land-sea interfaces as well as urban, forest, and farm land cover types. Figure 15 shows an RLSTAP generated terrain cover map of the CREST2 scene in polar format (range vs. angle). As in Figure 10, each concentric ring on the map in Figure 15 represents a 10 km increment where the center of the rings represents the location of the radar platform. For this example the maximum operational range is 145 km which is less than the maximum unambiguous range for the radar. The large arrow in the center of

Table 6. CREST2 Platform and Clutter Parameters

Parameter	Value
latitude	38.25° North
longitude	74.91° West
altitude	6.096 km
velocity	83.375 m/s
heading	10° GCS
mechanical boresight Azimuth	280° GCS
mechanical boresight Elevation	+2.5° (down)
recording start range	7 km
no. range samples	920
clutter scenario	Delmar MD, 38.46° N. , 75.58° W.
terrain spatial backscatter fluctuations	exponential
terrain temporal backscatter fluctuations	nonfluctuating
sea spatial backscatter fluctuations	exponential
sea temporal backscatter fluctuations	nonfluctuating
season	autumn
sea state	1
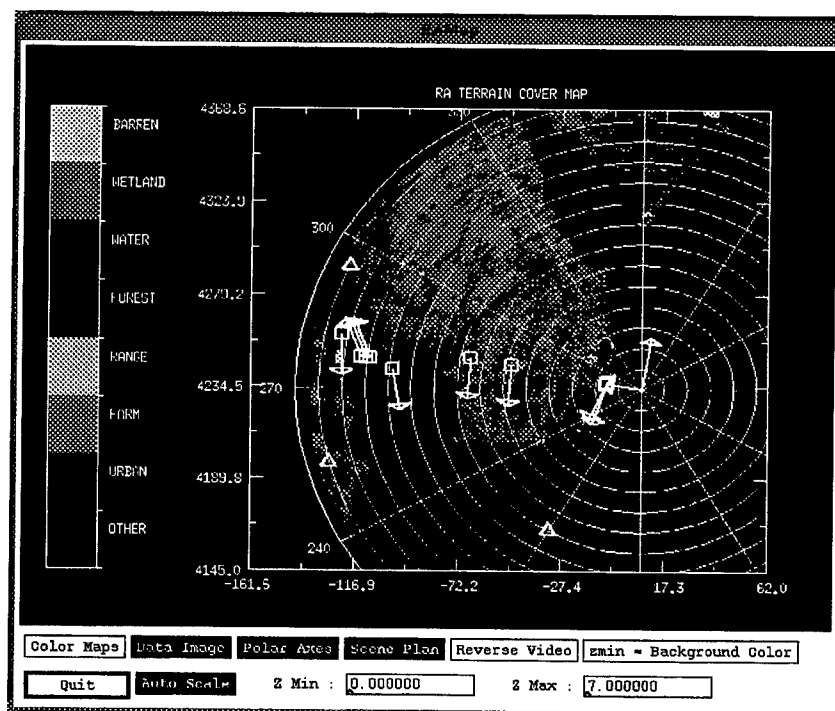
Fig. 15. Terrain Cover Map for CREST2.

the range rings represents the platform heading while the mechanical boresight of the antenna is represented by the small arrow.

Target locations in Figure 15 are represented by small squares with the target heading represented by the small arrow emanating from the square. Jammer locations are identified by small triangles. As can be seen, there are 9 targets and 3 jammers in this scenario. Specific signal parameters for CREST2 are given in Table 7. All targets for this example were placed to lie approximately within the 3 dB transmit beamwidth in both azimuth and elevation so that all have the possibility of being detected given that each lie within the mainbeam. However, target locations in angle/Doppler space were expected to cause detection problems following processing. One example is targets close to main beam clutter in terms of angle and Doppler where they may be adaptively canceled along with the clutter (targets 1 thru 5, and 9). A second example is targets in identical range/Doppler cells separated by less than or equal to the radar 3 dB azimuth beamwidth which challenges angle resolution [2] (target 1 and target 2). And thirdly, targets in the same angle/Doppler cell but different range cells (target 3, target 4, and targets 6 thru

Table 7. CREST2 Signal Scenario

Signal	Range,km (bin no.)	Az.	Dop.,Hz (bin no.)	snr,dB
thermal noise	-	-	-	53.7
clutter to noise	-	-	-	71.8
target 1	15.43 (57)	−2.5°	-150.2 (16)	-0.37
target 2	15.43 (57)	2.5°	-150.2 (16)	4.63
target 3	57.83 (340)	1.37°	100.2 (3)	-16.2
target 4	75.38 (457)	1.37°	100.1 (3)	-0.79
target 5	108.56 (678)	−5.0°	87.4 (3)	-12.2
target 6	118.89 (747)	−2.88°	-422.8 (11)	-12.0
target 7	120.74 (759)	−2.88°	-422.8 (11)	-12.26
target 8	122.59 (772)	−2.88°	-422.8 (11)	-12.52
target 9	132.46 (838)	1.37°	100.1 (3)	-10.71
jammer 1	140	15.0°	-	60.10
jammer 2	140	−25.0°	-	73.62
jammer 3	80	−70.0°	-	63.79

CLUTTER INTENSITY MAP

dB
-86.33
-122.75
-159.11
-195.47
-231.83
-268.19
-304.55
-340.92
-377.28
-413.64
-450.00

4368.61
4323.00
4279.18
Y (km) 4234.47
4189.76
4145.05

300
270
240

-161.50   -116.07   -72.16   -27.45   17.26   61.90
X (km)

Color Maps   Overlays   Labels   Annotate   Misc.
Quit   Zoom   Auto Scale   Z Min : -450   Z Max : -86.386
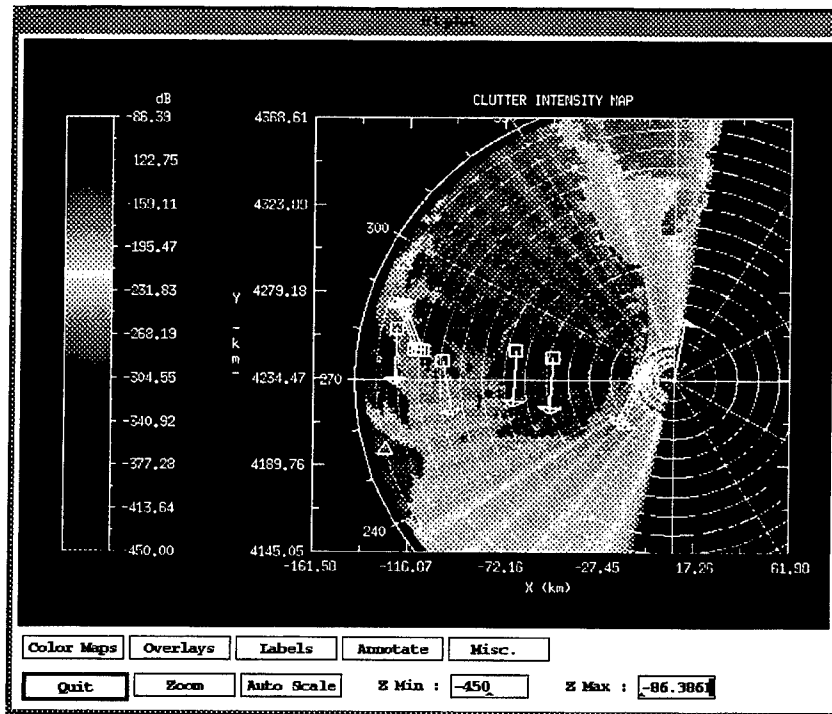
Fig. 16. Clutter Intensity Map for CREST2.

8) which can contaminate the training data with similar target information.

Because the clutter scene contains varying clutter types, finding appropriate training data for a given test cell was expected to be a challenge. Figure 16 shows a range-angle plot of the clutter intensity from the Delmar peninsula area as seen by the radar. The map indicates the many land sea interfaces that occur throughout the scene. The map also indicates that the only erratic clutter variation occurs between land and sea and that the land clutter is generally regular and benign. Note that the Virginia portion of the *peninsula* is missing. This is a known bug in RLSTAP dealing with naming conventions of USGS data and is being corrected. A scene plan is overlaid to indicate the locations of each target and jammer.

Figure 17 is a plot of the power of the CREST2 spectrum at range cell 457 in which target 4 lies. For a change of pace the platform velocity was set to induce a clutter ridge of slope .5 which can be seen in Figure 17. The three white noise barrage jammers are

43
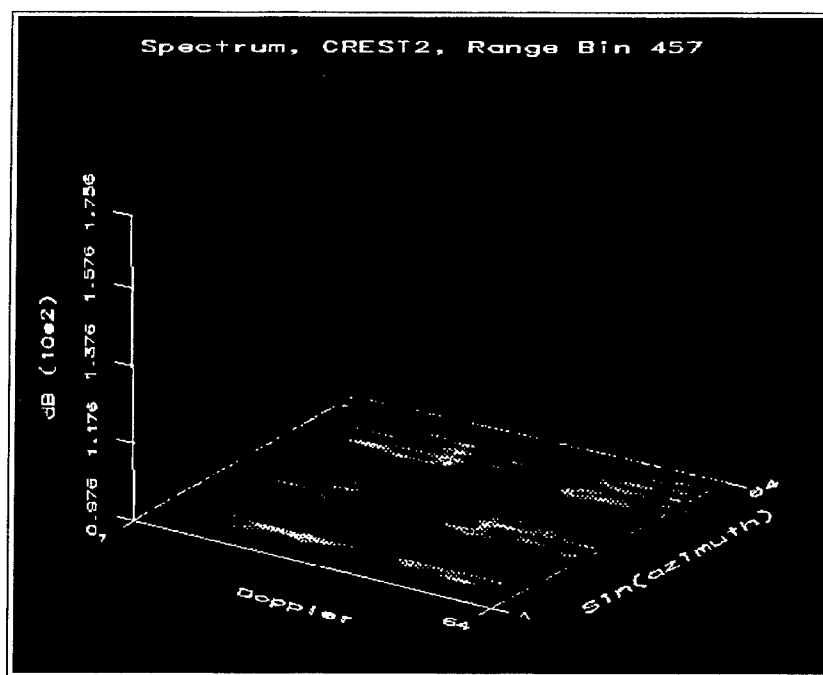
Fig. 17. Data Spectrum of CREST2, Range Cell 457.

clearly seen as they span all Doppler for three discrete angles. However, the target signal of target 4 is not detectable.

5.2 CREST2 Processing Results

The first approach taken for determining target detections was to use conventional processing techniques. Table 8 lists the conventional processing parameters used in processing CREST2. Note that the spatial steering vector was pointed in the same direction as the transmit beam which was pointed along the mechanical boresight. The resulting output power in a range-Doppler plot is shown in Figure 18. Indicated on the figure are the locations of possible targets in range and Doppler. Obviously none of the targets are visible. One may note that MTI was not applied to the data set before beamforming. Results have shown that when the main beam clutter is suppressed with MTI filtering, the jamming energy coming through the sidelobes, especially jammer 1 which enters the

44

Table 8. Conventional Beamforming, CREST2

Parameter	Description
pulse compression	LFM(50 μsec, 0.5 MHz), rectangular weight
motion compensation	none
MTI	none
Doppler filtering	Hamming wgt.
steering vector spatial az. weight	80 dB Chebyshev
steering vector spatial el. weight	rectangular
CFAR	none
pfa	none
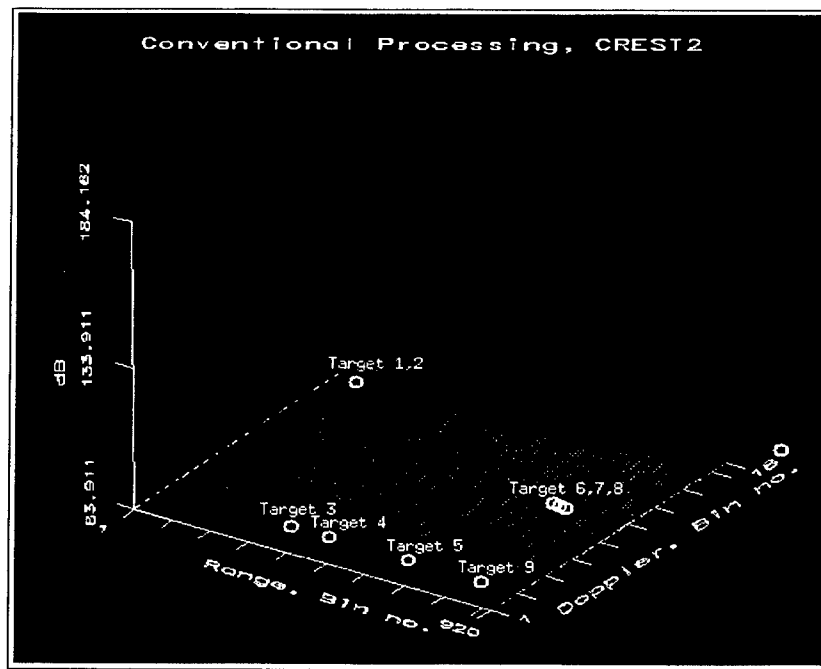
Fig. 18. Conventional Processing Applied to CREST2.

second sidelobe of the receive pattern steered to 0° in azimuth, saturates the Doppler spectrum making the output virtually useless.

For adaptive processing a partially adaptive two-pulse ADPCA algorithm was chosen. Table 9 lists the parameters used when CREST2 was processed using the two-pulse AD-PCA algorithm. Note that the spatial steering vector was pointed in the same direction

45

Table 9. ADPCA Processing, CREST2

Parameter	Description
pulse compression	LFM(50 μsec, 0.5 MHz), rectangular weight
training range cells (no.)	80 - 280
guard cells (no.)	none
no. of pulses	2
diagonal loading (w/r peak)	-55 dB
steering vector spatial az. weight	Hamming
steering vector spatial el. weight	rectangular
steering vector temporal weight	$[1, -1]$
Doppler filtering	80 dB Chebyshev
CFAR	cell averaging, 20 bins
pfa	10^{-6}

as the transmit beam which was pointed along the mechanical boresight.

The data was first pulse compressed prior to ADPCA processing. For the two-pulse ADPCA algorithm, the DOF required are $K = 2N = 40$. This suggests at least $2K = 80$ data snapshots be used in the covariance estimate and for this example the requirement was exceeded. After a small amount of diagonal loading was applied to the covariance estimate, one adaptive weight vector was found and applied to the entire CPI. Doppler processing followed filtering. The result is shown in Figure 19. All targets are visible in the range-Doppler domain. For the observation of targets 1 and 2, which are in the same range-Doppler cell but separated in angle, a range-angle plot would be necessary to distinguish both targets, however, one is not shown here.

A majority of the targets can be visually spotted in Figure 19. However, there are several other anomalies which could be considered to be targets. For this reason the output from Doppler processing was passed through a cell averaging CFAR process with a 20 bin averaging window and a pfa $= 10^{-6}$. The resulting detection map is shown in Figure 20. All targets are detectable after CFAR processing.
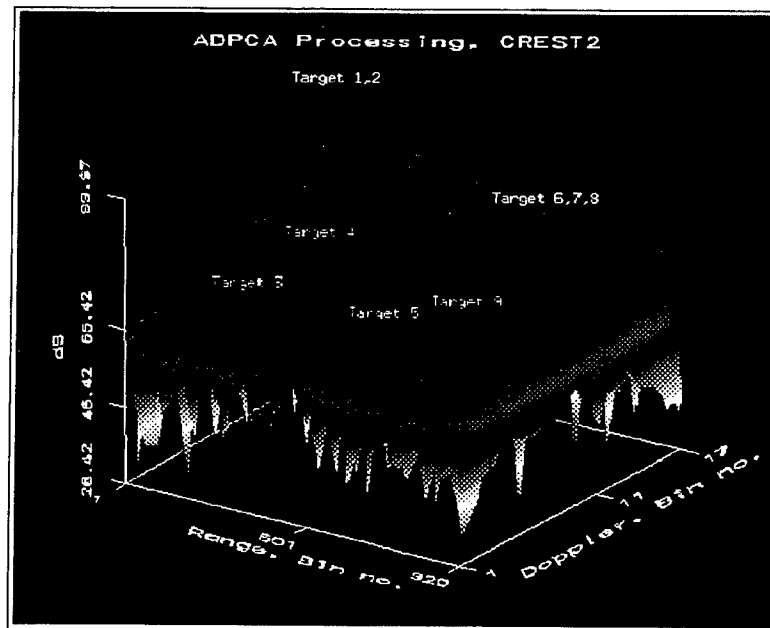
46

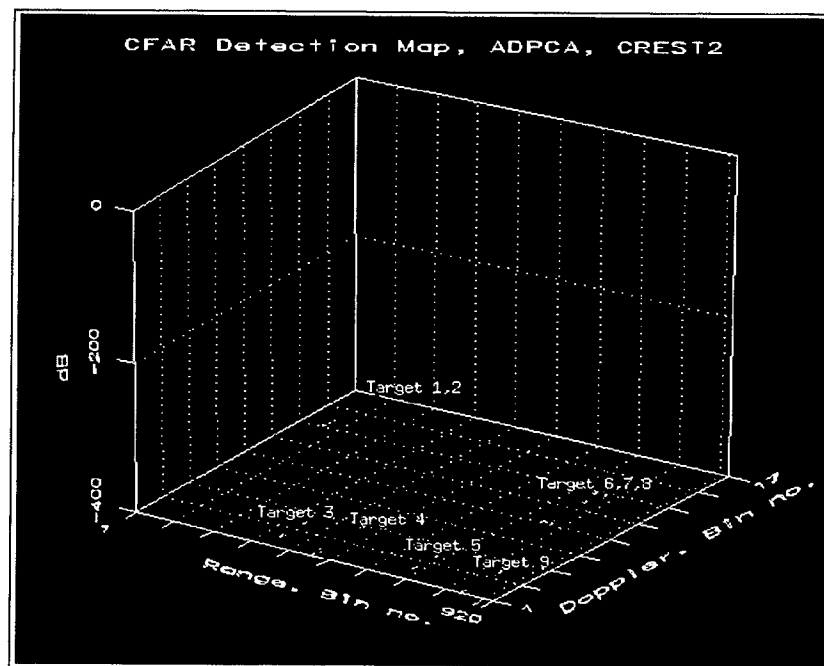Fig. 19. Two-pulse ADPCA Processing Applied to CREST2.

Fig. 20. Two-pulse ADPCA Processing Followed by Cell Averaging CFAR
Performed on CREST2, pfa=10^{-6}.

47

6   Data Set 3 - CREST3

The third data set of the challenge, CREST3, was installed on the CREST homepage in early July 1996. As with CREST2 this data set was given to the challengers with no specific information about target or jammer locations. Site specific clutter was used to provide a challenging and realistic clutter scenario for this data set. The radar platform was positioned near the city of Olympia, Washington. This area provides a suitable variation in ground cover type and backscatter strength to be a challenge in finding appropriate training data.

6.1   Overview

For this data set the airborne platform was at an altitude of 20,000 feet heading in a northwesterly direction. The antenna mechanical boresight was pointed slightly east of true North in azimuth, 60° clockwise from the heading vector. In elevation the mechanical boresight was pointed down 2.5°. The velocity of the platform was chosen such that the slope of the clutter ridge is $\beta = 1$. Specific information about platform parameters as well as information about the clutter scenario is given in Table 10.

The site specific clutter map for this data set was centered about the city of Olympia, Washington (47.05° N., 122.89° W.) The platform location was slightly south of the center of the map. This clutter site provides a variety of clutter types including urban, forest, sea, and mountains. As with CREST2, this set provides a challenge in finding appropriate secondary data for covariance estimation. Figures 21, 22, and 23 provide the terrain cover map, terrain height map, and clutter intensity map for the Olympia Washington area. The maximum operational range for the radar was set to 145 km which is evident in the maps. For this particular scene those things indicated in Figure 21 as *Range* are mountains. Because of these mountains and given the geometry of the platform, some of the clutter returns produce zero backscatter due to the line-of-sight blockage from the mountains. If one compares Figures 22 and 23 there is a correlation between the

Table 10. CREST3 Platform and Clutter Parameters

Parameter	Value
latitude	46.65° North
longitude	122.89° West
altitude	6.096 km
velocity	166.7 m/s
heading	−40° GCS
mechanical boresight Azimuth	20° GCS
mechanical boresight Elevation	+2.5° (down)
recording start range	7 km
no. range samples	920
clutter scenario	Olympia WA, 47.05° N., 122.89° W.
terrain spatial backscatter fluctuations	Weibull
terrain temporal backscatter fluctuations	nonfluctuating
sea spatial backscatter fluctuations	exponential
sea temporal backscatter fluctuations	nonfluctuating
season	autumn
sea state	1

mountainous areas and those areas from which the radar does not receive a return. This can cause a problem in training data selection if a target were to lie above one of these *blocked out* areas. However, this is not the case here as the main beam is pointed along the Puget Sound where there are still varying backscatter strengths due to the many land-sea interfaces but few line of sight blockage problems. Although, clutter returns are a sum of all clutter backscatter (or lack of backscatter due to line-of-sight blockage) contained in an entire range cell surrounding the platform weighted by the antenna 3-dimensional beam pattern. Therefore for this example, the blocked portions of clutter in the sidelobes of the main beam will still effect the value of the returns in both the primary and secondary data.

Another clutter phenomena to be aware of is the frequency shift imparted on the clutter ridge due to the angle misalignment between the heading vector and mechanical boresight. This can be thought of as a simulated form of crab angle where the array is typically thought to be perpendicular to the heading vector. Because the angle between
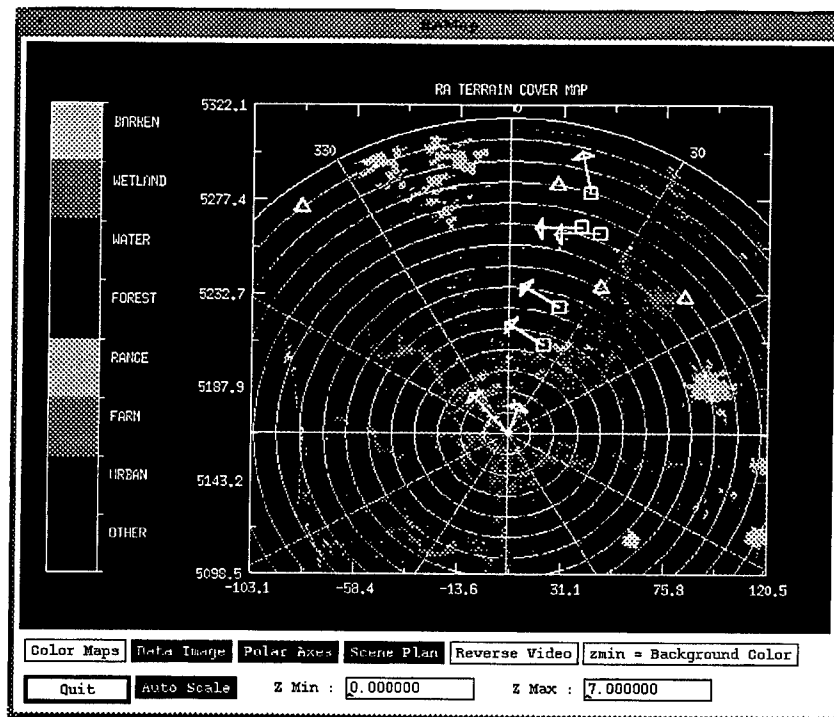
Fig. 21. Terrain Cover Map for CREST3.
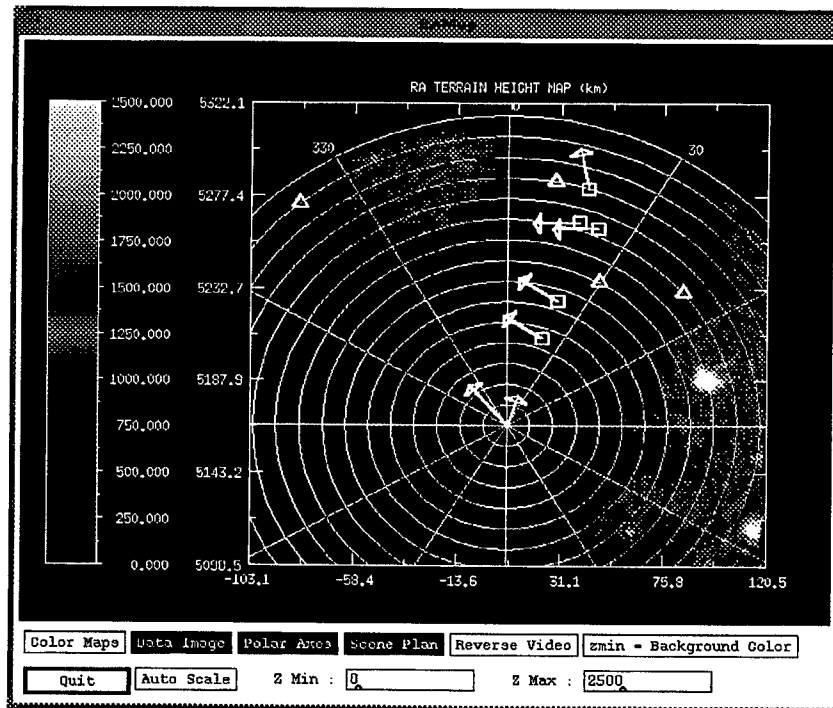
Fig. 22. Terrain Elevation Map for CREST3.

50
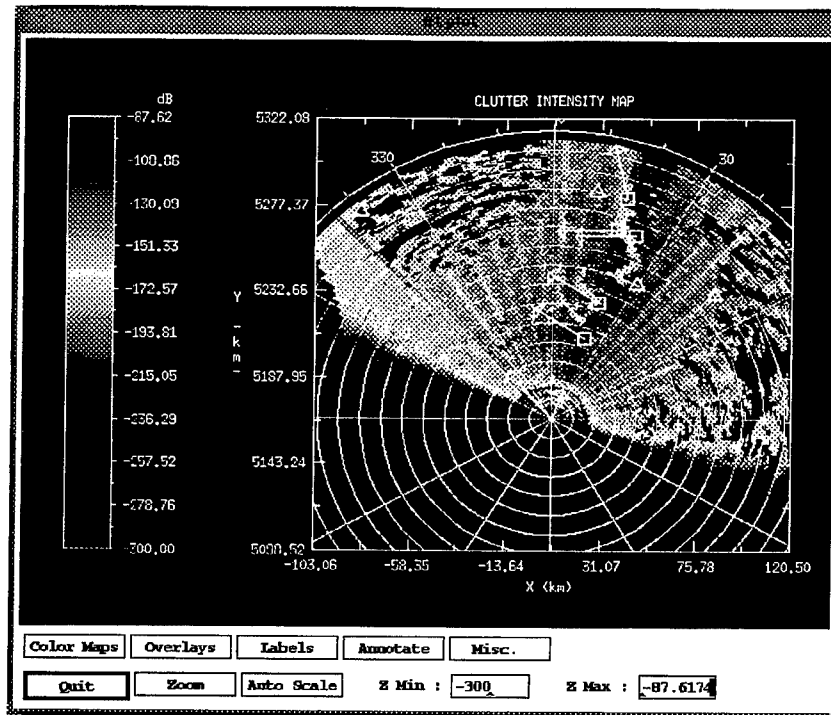
Fig. 23. Clutter Intensity Map for CREST3.

the heading vector and boresight is 60°, the clutter ridge will incur a frequency shift in Doppler as well as take on a slight elliptical shape [10]. If one is to apply MTI to this radar data, motion compensation should be used first to account for the frequency shift.

As seen in Figures 21, 22, and 23, a scene plan has been overlaid which depicts the target and jammer geometry. Table 11 gives specific parameter information on each target and jammer as well as the thermal noise and clutter signal-to-noise ratio. The targets were all placed approximately within the 3 dB azimuth and elevation beamwidth of the antenna which is pointed along the Puget Sound. Furthermore, targets 1 and 2 (see Table 11) were placed in the same angle/Doppler cell, separated in range so as to cause possible signal contamination in the training data. Targets 3 and 4 were placed in same range Doppler cell and separated by a beamwidth. Most targets in CREST3 were placed close to main beam clutter in terms of Doppler and angle to create the possibility of target elimination along with main beam clutter cancellation.

51

Table 11. CREST3 Signal Scenario

Signal	Range,km (bin no.)	Az.,deg	Dop.,Hz (bin no.)	snr,dB
thermal noise	-	-	-	53.7
clutter to noise	-	-	-	74.36
target 1	44.52 (251)	0.00	105.2 (3)	-13.78
target 2	64 (381)	0.00	105.5 (3)	-9.84
target 3	103 (641)	−2.50	458.19 (9)	-13.34
target 4	103 (641)	2.50	458.19 (9)	-11.35
target 5	119.5 (751)	−3.00	-450.8 (11)	-16.44
jammer 1	140	−60.00	-	72.93
jammer 2	120	−10.00	-	75.23
jammer 3	80	10.00	-	74.33
jammer 4	100	30.00	-	80.77

All the jammers are white noise barrage jammers. Two of the jammers, jammers 2 and 3, were placed 10° off from the main beam. These two jammers could have a significant effect depending on the azimuth beamwidth of the receive beam.

Figure 24 displays the power spectrum of CREST3 for range cell 751. As can be seen, the four jammers *mask* any semblance of the clutter ridge and target 5, which is located in this range cell, is not detectable.

6.2 CREST3 Processing Results

Figure 25 displays the output result from conventional processing in range vs. Doppler. Pulse compression of CREST3 was followed by Doppler processing and nonadaptive beamforming. Table 12 lists all the pertinent parameters for conventional processing for this example. Note that the spatial steering vector was pointed in the same direction as the transmit beam which was pointed along the mechanical boresight.

The location of each target in range-Doppler space is indicated by a small circle in Figure 25. Note that none of the targets is easily identifiable. The main beam clutter energy, indicated by the dark line along Doppler bin 5, is shifted in frequency as expected due to the 60° crab angle. The main beam clutter Doppler frequency shift is calculated

52
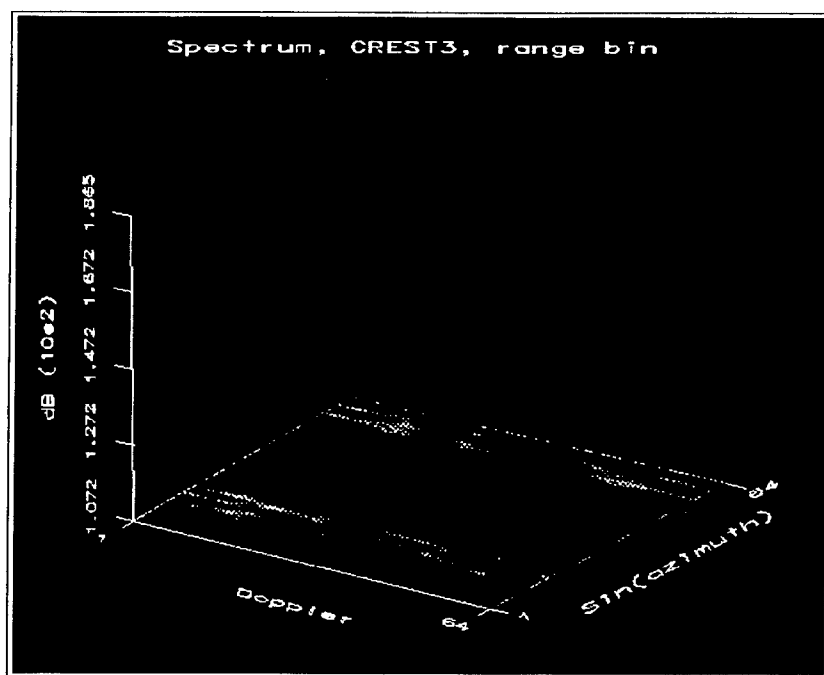
Fig. 24. Data Spectrum of CREST3, Range Cell 751.

Table 12. Conventional Beamforming, CREST3

Parameter	Description
pulse compression	LFM(50 μsec, 0.5 MHz), rectangular weight
motion compensation	none
MTI	none
Doppler filtering	Hamming weight
steering vector spatial az. weight	80 dB Chebyshev
steering vector spatial el. weight	rectangular
CFAR	none
pfa	none

by

$$f_c = \frac{2v}{\lambda} \cos(\theta_c) \cos(\phi_c). \tag{24}$$

Here θ_c is the elevation angle measured between boresight and the platform horizontal. The azimuth angle ϕ_c is measured between boresight and the heading vector of the aircraft. For this example $f_c = \frac{2(166.7)}{0.667} \cos(2.5°) cos(60°) \approx 250$ Hz.

53
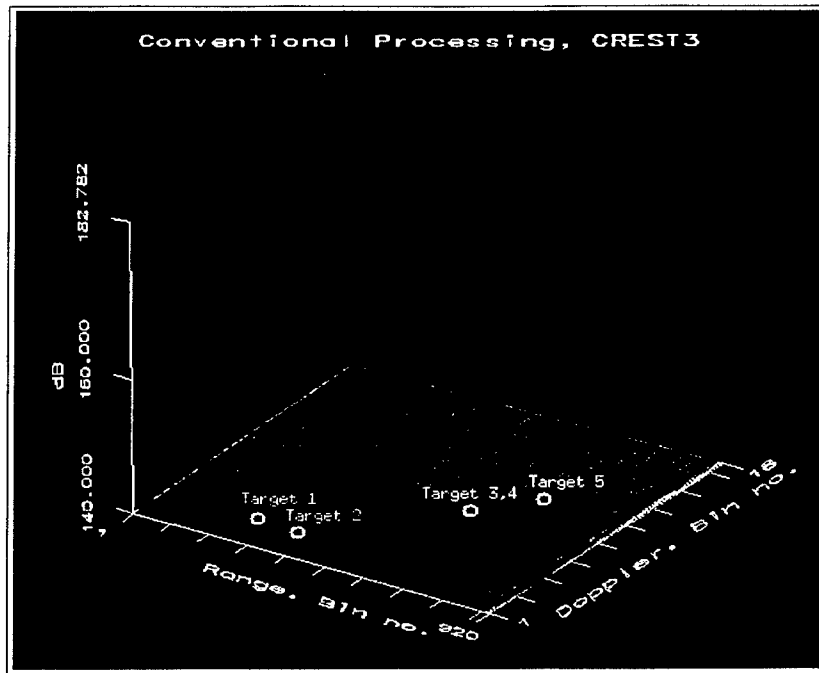
Fig. 25. Conventional Processing Applied to CREST3.

The partially adaptive FTS technique was also used to process CREST3. Pulse compression, motion compensation, and MTI filtering were used to preprocess the data before FTS algorithm was applied. Table 13 lists the parameters associated with processing CREST3 using the FTS algorithm. Note that the spatial steering vector was pointed in the same direction as the transmit beam which was pointed along the mechanical boresight.

Figure 26 shows the detection map after FTS processing and applying cell averaging CFAR to CREST3. The choice for training data for this example was somewhat arbitrary. The guard region was chosen to exclude targets 3 and 4 from the covariance estimate. As can be seen in Figure 26 only target 5 appears after processing. Other training strategies were used by choosing other training data and guard regions with equal or worse results as show here using the FTS algorithm. In each case the number of training samples equaled or exceeded the $2(DOF) = 2N = 40$ required samples.

54

Table 13. Factored Time-Space Processing, CREST3

Parameter	Description
pulse compression	LFM(50 μsec, 0.5 MHz), rectangular weight
motion compensation	250 Hz
MTI	3 pulse
Doppler filtering	80 dB Dolph Cheb.
training range cells (no.)	550 - 750
guard cells (no.)	631 - 651
diagonal loading (w/r peak)	-55 dB
steering vector spatial az. weight	Hamming
steering vector spatial el. weight	rectangular
CFAR	cell averaging, 50 bins
pfa	10^{-6}
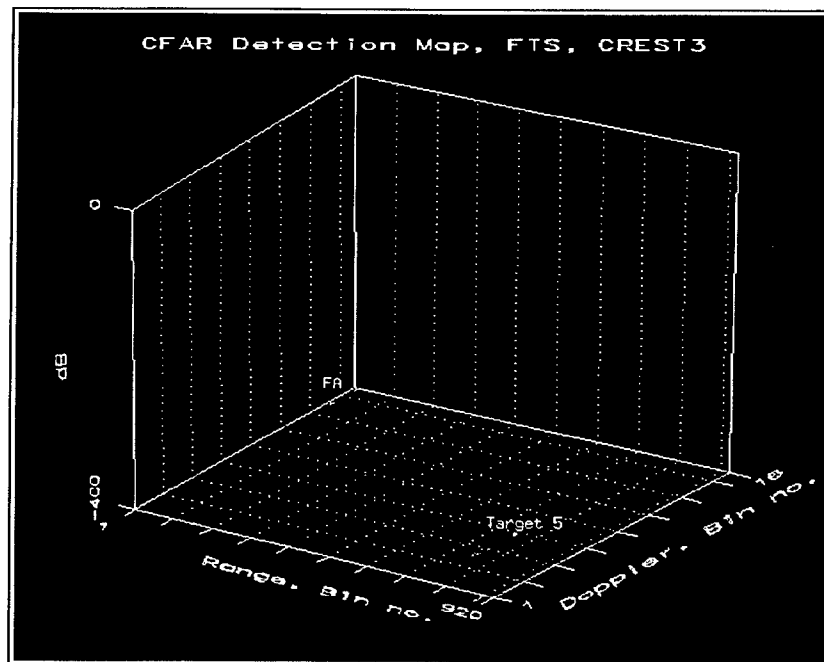
Fig. 26. Factored Time-Space Processing Followed by Cell Averaging CFAR Performed on CREST3, pfa= 10^{-6}.

Table 14. Adaptive Displaced Phase Center Array Processing, CREST3

Parameter	Description
pulse compression	LFM(50 μsec, 0.5 MHz), rectangular weight
motion compensation	250 Hz
training range cells (no.)	480 - 800
guard cells (no.)	631 - 651
no. of pulses	3
diagonal loading (w/r peak)	-50 dB
steering vector spatial az. weight	Hamming
steering vector spatial el. weight	rectangular
steering vector temporal weight	$[1, -2, 1]$
Doppler filtering	80 dB Chebyshev
CFAR	cell averaging, 50 bins
pfa	10^{-5}

An alternate approach was to use the three-pulse ADPCA algorithm. For this example ADPCA filtering was preceded by pulse compression and motion compensation and followed by Doppler filtering. Table 14 lists the particular processing values associated with this ADPCA processing example.

As with the FTS example, a similar guard region was used and only one adaptive weight vector was found and applied to all range snapshots in the CPI. After cell averaging CFAR, with a higher pfa than in the previous FTS example, the target detections shown in Figure 27 were the results. As can be seen several false alarms appear along with all targets.
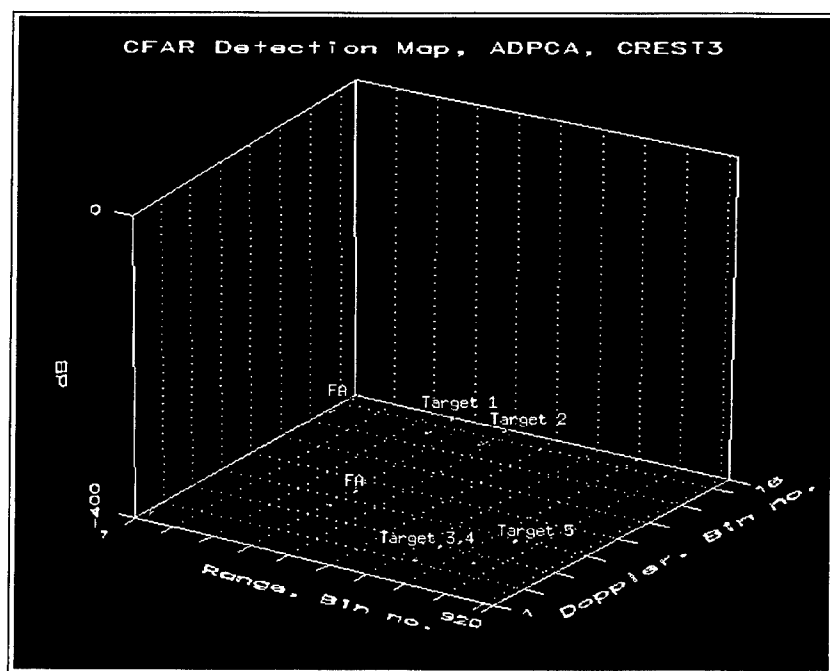
56

Fig. 27. Three-Pulse ADPCA Processing Followed by Cell Averaging CFAR
Performed on CREST3, pfa=10^{-5}.

7 Data Set 4 - CREST4

The fourth data set of the challenge, CREST4, was installed on the CREST homepage in early October 1996. The fourth data set actually consisted of 10 data sets named CREST41, CREST42,...CREST410. Each data set represents a consecutive CPI, or dwell, every 30 seconds as the radar boresight is pointed at a specific position on the ground. Site specific clutter from the Salt Lake City, Utah area make this set of data unique because of the wide varying terrain cover types.

7.1 Overview

The simulated airborne surveillance platform was heading in a straight path due North at constant velocity and altitude. The mechanical boresight of the array was adjusted every 30 seconds to point at a point of interest (POI) on the ground located West of the flight path (POI, 40.89° N., 112.61° W.) during the entire experiment. Table 15 lists the platform parameters as well as the clutter parameters for this example. At each interval a dwell lasting 18 pulses was sent and the range data samples collected between pulses, in each channel, represents one CPI. Figure 28 depicts the scene of CREST4 from CPI 1 to CPI 10. The objective was to have different target and jammer orientations relative to the platform from CPI to CPI. Each target was given a flight path so as to enter the main beam and provide some level of backscatter in at least one CPI. In this way targets are leaving and entering the search area of the radar as it flies, something that may actually happen in a realistic surveillance scenario. The jammers were fixed in range and azimuth relative to the heading vector of the platform. However, the jammer locations changed relative to the mechanical boresight of the radar from CPI to CPI causing various degrees of jammer energy to enter the radar through the main beam.

In order to implement the flying platform RLSTAP requires the position of the platform in latitude and longitude for each CPI. Given the platform starting position, velocity, revisit time between dwells (30 seconds), and path, values for the latitude and longitude
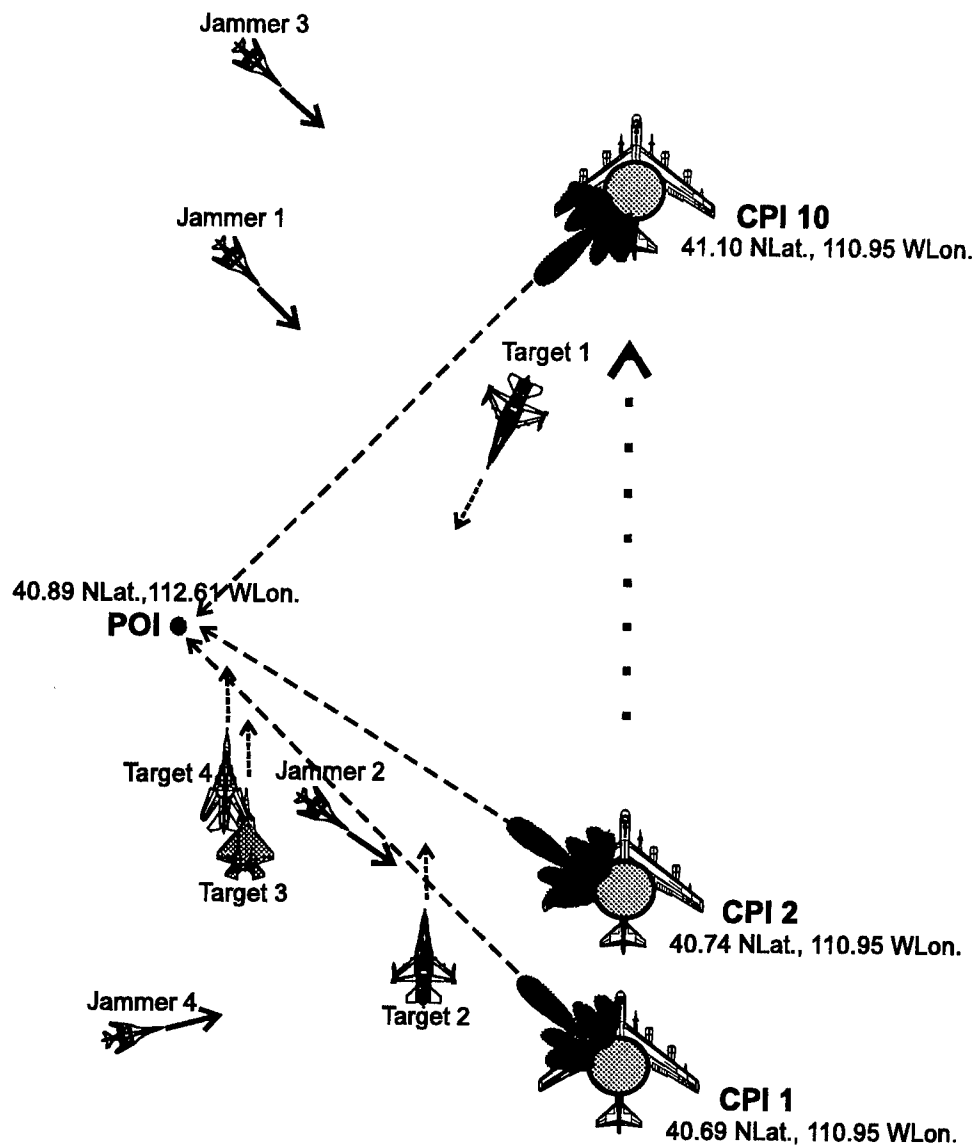
Fig. 28. CREST4 Scene Depiction From CPI 1 to CPI 10.

were calculated off-line and inserted into RLSTAP through the batch processing method described in Section 2.2. Another parameter that varied over the CPIs is the pointing direction of array boresight which was to remain fixed on the POI. This also was calculated off-line in terms of azimuth and elevation angles. The values of the platform location and mechanical boresight pointing angles are given in Table 16 for each CPI.

The clutter scene for this example is the Salt Lake City, Utah area. This site offers

59

Table 15. CREST4 Platform and Clutter Parameters

Parameter	Value
latitude	see Table 16
longitude	see Table 16
altitude	6.096 km
velocity	166.7 m/s
heading	0° GCS
mechanical boresight Azimuth	see Table 16
mechanical boresight Elevation	see Table 16
recording start range	7 km
revisit time between dwells	30 sec.
no. range samples	920
clutter scenario	Northeast Utah 41° N., 111.41° W.
terrain spatial backscatter fluctuations	Weibull
terrain temporal backscatter fluctuations	nonfluctuating
sea spatial backscatter fluctuations	exponential
sea temporal backscatter fluctuations	nonfluctuating
season	summer
sea state	1

Table 16. Platform Parameters per CPI.

CPI no.	Lat. deg. N	Lon. deg. W	Boresight Az. deg. GCS	Boresight El. deg. down
1	40.698	-110.95	-80.879	2.46
2	40.743	-110.95	-82.882	2.48
3	40.788	-110.95	-84.902	2.49
4	40.833	-110.95	-86.935	2.49
5	40.878	-110.95	-88.976	2.49
6	40.922	-110.95	-91.020	2.49
7	40.967	-110.95	-93.061	2.49
8	41.012	-110.95	-95.094	2.49
9	41.057	-110.95	-97.114	2.48
10	41.102	-110.95	-99.117	2.46

various cover types such as range land, farming areas, forest, mountains, and water. Figures 29, 30, and 31 show the terrain cover map, terrain height map, and clutter intensity map respectively for the 5th CPI of CREST4. The scene plan overlay on each figure indicate the positions of the 4 targets (identified by the small squares) and the 4 jammers (identified by the small triangles).

As can be seen on the clutter intensity map, Figure 31, there is a significant amount of line-of-sight blockage along the boresight direction due to mountainous regions. For this reason choosing secondary data is a challenge because some range cells used as training data may not be representative of the clutter found in the range cell under test. One potential problem is choosing secondary data for the furthest two targets from the radar, targets 3 and 4. These two targets *fly* along an edge of clutter/no clutter return area. It is often customary to choose secondary data from neighboring range cells about the cell under test. In this particular case cells used in the no clutter region will adversely effect the covariance estimate while cells in the clutter region may be appropriate training cells.

Because of the geometry of the CREST4 data set not every target is detectable in every CPI due to its location in azimuth and/or Doppler. Figure 32 shows the location of each target in azimuth (GCS) from CPI 1 to CPI 10. As a reference, the mechanical boresight azimuth is also shown. The symbols indicated above and below the boresight line by the * symbol represent the 3 dB beamwidth (5°) of the main beam about the boresight line. The return power level from a target depends on a number of variables including, range to target, radar cross section, and antenna gain in the direction of the target. Obviously, targets outside the 3 dB beamwidth of the main beam incur significant attenuation and become difficult to detect. As will be shown with processing examples, no true target detections are seen until CPI 4 and this is supported by Figure 32 where target 2 is shown to be the first target to become close to the main beam at that time.

Targets also compete with main beam clutter. If targets fall close to main beam clutter in Doppler, they have an improved chance of being canceled along with the clutter.
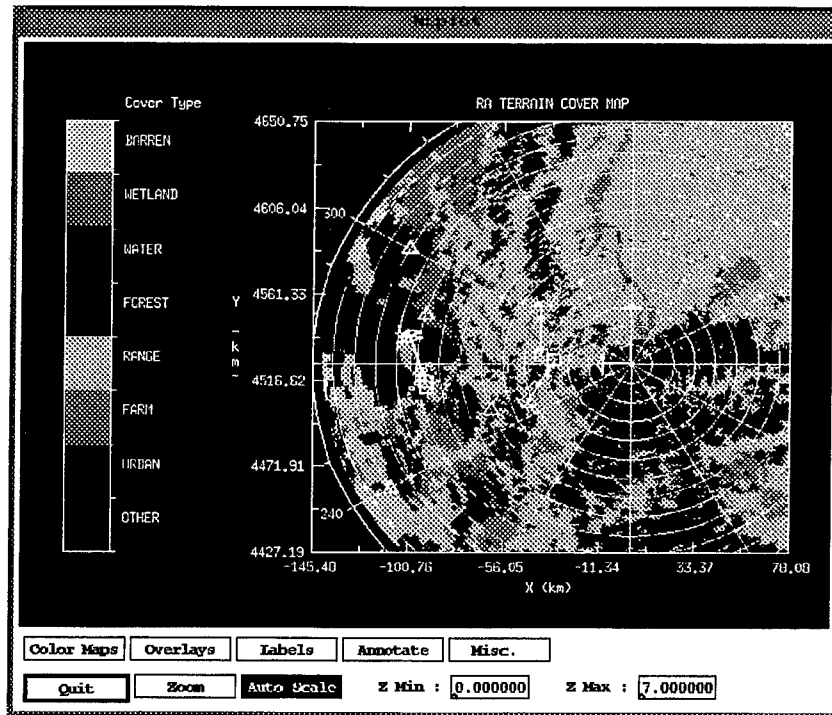
Fig. 29. Terrain Cover Map for CREST4 CPI 5 (CREST45).
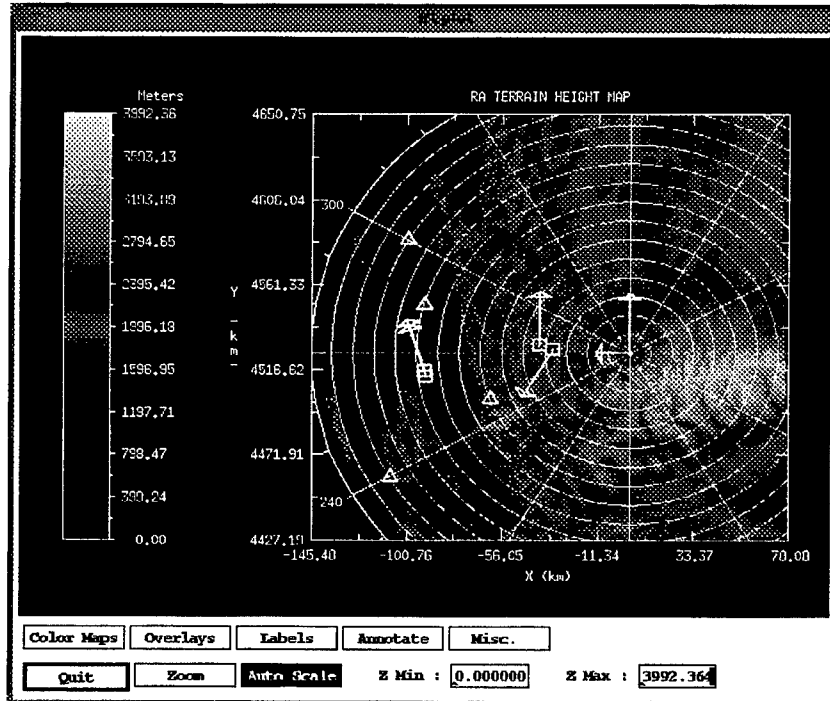
Fig. 30. Terrain Elevation Map for CREST4 CPI 5 (CREST45).
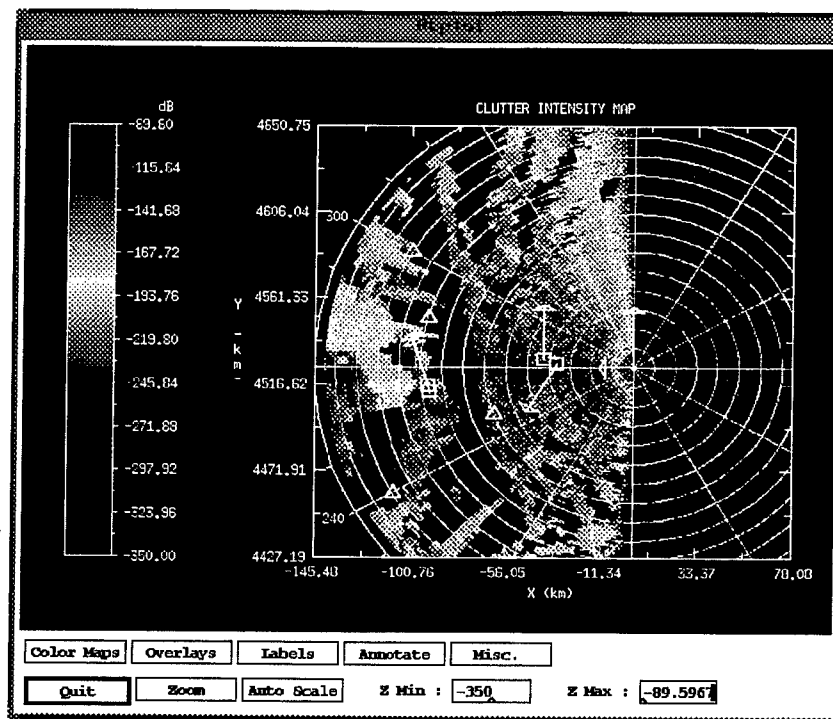
Fig. 31. Clutter Intensity Map for CREST45.
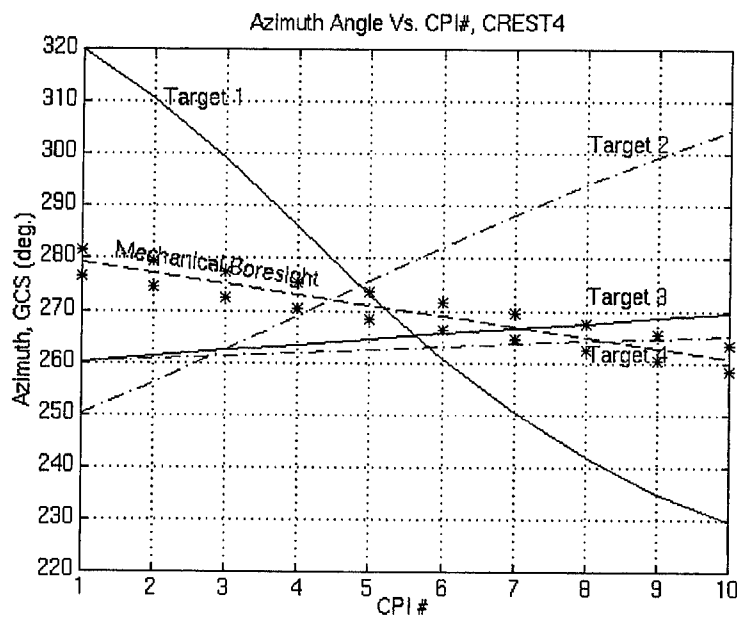
Fig. 32. Target Azimuth and Mechanical Boresight Azimuth Relative to True North vs. CPI Number.

63
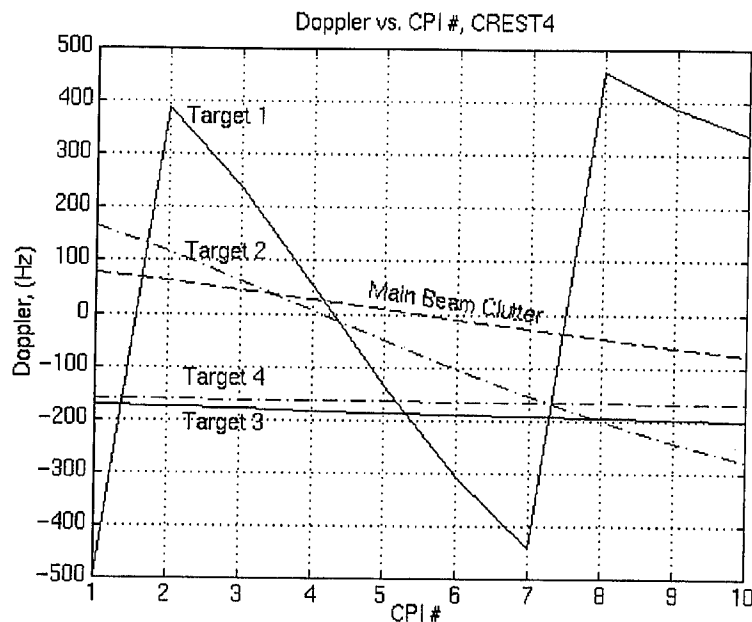
Fig. 33. Target Doppler and Main Beam Clutter Doppler vs. CPI Number.

Figure 33 gives the target's Doppler vs. CPI number. Also plotted is the main beam clutter Doppler. Obviously a target must be in the 3 dB beamwidth of the main beam and have a Doppler frequency close to that of the main beam clutter in order to be canceled or obscured by main beam clutter. One example of this occurrence is target 2 during CPI 5. During this instance target 2 is just outside the 3 dB beamwidth and the Doppler difference between it and the main beam clutter is approximately 55 Hz which could put both the main beam clutter and the target in a clutter null after processing.

Tables 17, 18, 19, and 20 list the signal parameters for both targets and jammers in each of the 10 CPI's. Clutter and thermal noise powers are given as well.

Table 17. CREST4 Signal Scenario for CPI 1 - CPI 3

Signal	Range,km (bin no.)	Az.,deg	Dop.,Hz (bin no.)	snr,dB
CPI 1				
thermal noise	-	-	-	53.7
clutter to noise	-	-	-	70.06
target 1	45 (254)	40.77°	504.95 (10)	-30.64
target 2	45.08 (255)	−29.05°	166.97 (4)	2.08
target 3	90.19 (556)	−19.08°	-171.07 (16)	-26.25
target 4	90.19 (556)	−19.08°	-160.04 (16)	-16.25
jammer 1	100	5.88°	-	76.89
jammer 2	70	−29.12°	-	74.18
jammer 3	120	20.88°	-	72.84
jammer 4	130	−39.12°	-	81.22
CPI 2				
thermal noise	-	-	-	53.7
clutter to noise	-	-	-	70.69
target 1	40.52 (225)	33.38°	390.34 (8)	-25.95
target 2	43.60 (245)	−21.01°	117.63 (3)	12.11
target 3	91.84 (567)	−15.87°	-175.07 (16)	-25.61
target 4	91.72 (566)	−16.43°	-161.19 (16)	-19.17
jammer 1	100	7.88°	-	77.20
jammer 2	70	−27.12°	-	74.15
jammer 3	120	22.88°	-	73.23
jammer 4	130	−37.12°	-	81.31
CPI 3				
thermal noise	-	-	-	53.7
clutter to noise	-	-	-	72.13
target 1	37.38 (204)	24.06°	238.38 (5)	-31.38
target 2	42.64 (239)	−12.61°	64.05 (2)	10.66
target 3	93.53 (578)	−12.69°	-178.86 (16)	-27.47
target 4	93.27 (576)	−13.78°	-162.29 (16)	-12.36
jammer 1	100	9.90°	-	77.41
jammer 2	70	−25.10°	-	74.00
jammer 3	120	24.90°	-	73.34
jammer 4	130	−35.10°	-	81.24

Table 18. CREST4 Signal Scenario for CPI 4 - CPI 6

Signal	Range,km (bin no.)	Az.,deg	Dop.,Hz (bin no.)	snr,dB
CPI 4				
thermal noise	-	-	-	53.7
clutter to noise	-	-	-	70.47
target 1	35.92 (194)	13.28°	55.67 (2)	-16.86
target 2	42.22 (236)	−3.99°	7.87 (1)	25.85
target 3	95.26 (590)	−9.54°	-182.44 (16)	-20.16
target 4	94.83 (587)	−11.14°	-163.33 (16)	-18.15
jammer 1	100	11.93°	-	77.58
jammer 2	70	−23.06°	-	73.81
jammer 3	120	26.94°	-	73.38
jammer 4	130	−33.06°	-	81.12
CPI 5				
thermal noise	-	-	-	53.7
clutter to noise	-	-	-	66.72
target 1	36.34 (197)	2.12°	-135.14 (17)	0.820
target 2	42.37 (237)	4.69°	-48.77 (18)	20.87
target 3	97.02 (601)	−6.42°	-185.83 (16)	-24.40
target 4	96.40 (597)	−8.51°	-164.32 (16)	-8.14
jammer 1	100	13.98°	-	77.79
jammer 2	70	−21.02°	-	73.65
jammer 3	120	28.98°	-	73.54
jammer 4	130	−31.0°	-	81.07
CPI 6				
thermal noise	-	-	-	53.7
clutter to noise	-	-	-	67.56
target 1	38.59 (212)	−8.09°	-306.31 (13)	-11.96
target 2	43.08 (242)	13.23°	-103.64 (17)	14.78
target 3	98.81 (613)	−3.33°	-189.04 (16)	-10.20
target 4	97.97 (608)	−5.9°	-165.26 (16)	-13.48
jammer 1	100	16.02°	-	77.99
jammer 2	70	−18.98°	-	73.50
jammer 3	120	31°	-	73.71
jammer 4	130	−28.98°	-	81.03

Table 19. CREST4 Signal Scenario for CPI 7 - CPI 9

Signal	Range,km (bin no.)	Az.,deg	Dop.,Hz (bin no.)	snr,dB
CPI 7				
thermal noise	-	-	-	53.7
clutter to noise	-	-	-	66.31
target 1	42.37 (237)	−16.54°	-441.94 (11)	-27.02
target 2	44.32 (250)	21.49°	-154.86 (16)	10.78
target 3	100.63 (625)	−0.285°	-192.07 (16)	-5.01
target 4	99.56 (618)	−3.31°	-166.16 (16)	-0.28
jammer 1	100	18.06°	-	78.22
jammer 2	70	−16.94°	-	73.38
jammer 3	120	33.06°	-	73.98
jammer 4	130	−26.94°	-	81.04
CPI 8				
thermal noise	-	-	-	53.7
clutter to noise	-	-	-	68.4
target 1	47.32 (270)	−23.04°	-541.57 (9)	-38.63
target 2	46.04 (261)	29.33°	-201.13 (15)	-0.28
target 3	102.47 (638)	−2.72°	-194.94 (15)	-8.98
target 4	101.15 (629)	−0.75°	-167.02 (16)	4.85
jammer 1	100	20.10°	-	78.40
jammer 2	70	−14.91°	-	73.20
jammer 3	120	35.09°	-	74.13
jammer 4	130	−24.91°	-	80.96
CPI 9				
thermal noise	-	-	-	53.7
clutter to noise	-	-	-	67.52
target 1	53.11 (309)	−27.81°	-612.42 (8)	-30.08
target 2	48.21 (276)	36.70°	-241.84 (15)	-5.47
target 3	104.35 (650)	5.67°	-197.65 (15)	-23.87
target 4	102.74 (639)	1.79°	-167.83 (16)	3.22
jammer 1	100	22.11°	-	78.54
jammer 2	70	−12.89°	-	72.99
jammer 3	120	37.11°	-	74.21
jammer 4	130	−22.89°	-	80.85

Table 20. CREST4 Signal Scenario for CPI 10

Signal	Range,km (bin no.)	Az.,deg	Dop.,Hz (bin no.)	snr,dB
CPI 10				
thermal noise	-	-	-	53.7
clutter to noise	-	-	-	65.43
target 1	59.50 (351)	−31.21°	-662.62 (7)	-39.30
target 2	50.75 (293)	43.54°	-276.95 (14)	-14.24
target 3	106.25 (663)	8.58°	-200.22 (15)	-19.88
target 4	104.35 (650)	4.30°	-168.61 (16)	-7.10
jammer 1	100	24.12°	-	78.68
jammer 2	70	−10.88°	-	72.76
jammer 3	120	39.11°	-	74.30
jammer 4	130	−20.88	-	80.74

7.2 CREST4 Processing Results

In this section several processing results will be given to indicate the presence of targets in some of the CPIs contained in the data set CREST4. Because of time constraints and the brevity of this report nonexhaustive trial and error approaches were used in choosing algorithm parameters in order to yield sufficient results. All four algorithms discussed in Section 3 were applied to every CPI using somewhat crude training approaches. All adaptive weight training was based on the *freeze training* approach where one adaptive weight vector was found with one set of training data and applied to both the primary and secondary (training) data. For all results shown here the spatial steering vector azimuth and elevation angles were set to zero so that the receive beam is formed in the same direction as the mechanical boresight (which is the same direction as the transmit waveform). The best results, in terms of the number of targets detected, from the algorithm comparisons will be given here.

As can be seen in Figure 32, none of the four targets approach the vicinity of the main beam until CPI 4. The processing of data file CREST44.dat(mat) (data file for CPI 4) was the first report of any meaningful result. The best results were received from using a two pulse ADPCA algorithm. ADPCA filtering was preceded by pulse compression and motion compensation. Motion compensation was used on all CPIs prior to adaptive processing to account for the slight crab angle incurred because of the misalignment between the platform heading and the mechanical boresight. The amount of compensation is calculated using (24) and the values for mechanical boresight azimuth and elevation given in Table 16. After applying two pulse ADPCA filtering to CREST44, cell averaging CFAR was used to detect target 2. The resulting detection map is given in Figure 34. All algorithm and processing parameters for this example are given in Table 21.

Figure 32 indicates that at least one target in CPI 5 thru CPI 10 will intersect with the radar main beam above or near the 3 dB point. CPI 5, CREST45.dat(mat), was processed with the processing approaches described in Section 3. The FTS, ADPCA,

Table 21. Adaptive Displaced Phase Center Array Processing, CREST44

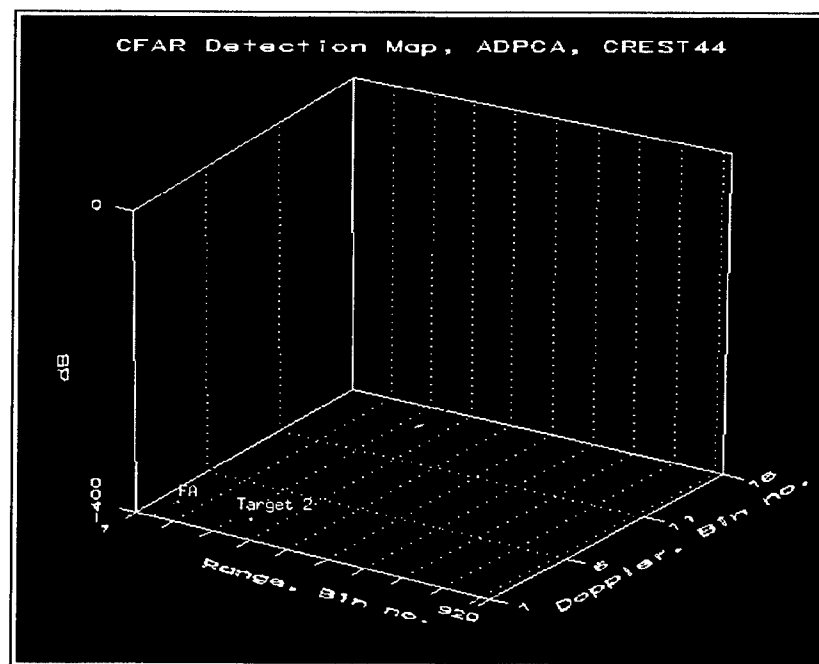| Parameter	Description
pulse compression	LFM(50 μsec, 0.5 MHz), rectangular weight
motion compensation	26.7 Hz
training range cells (no.)	1-800
guard cells (no.)	none
no. of pulses	2
diagonal loading (wrt peak)	-50 dB
steering vector spatial az. weight	Hamming
steering vector spatial el. weight	rectangular
steering vector temporal weight	$[1, -1]$
Doppler filtering	80 dB Chebyshev
CFAR	cell averaging, 40 bins
pfa	10^{-6}

Fig. 34. Two Pulse ADPCA Processing Followed by Cell Averaging CFAR Performed on CREST44, pfa= 10^{-6}.

Table 22. Joint Domain Processing, CREST45

Parameter	Description
pulse compression	LFM(50 μsec, 0.5 MHz), Hamming weight
training range cells (no.)	1 - 850
guard cells (no.)	none
diagonal loading (wrt peak)	-55 dB
steering vector spatial az. weight	Hamming
steering vector spatial el. weight	rectangular
steering vector temporal weight	Hamming
CFAR	cell averaging, 40 bins
pfa	10^{-6}

and JD approaches all were able to produce detections of targets 1 and 2. The JD algorithm performed well with given training strategies to yield no false alarms. JD filtering was preceded by pulse compression. Because of the size of the array and the number of pulses used, the JD process requires at least $2NM = 720$ training samples for covariance estimation. For this example 850 training samples were used. JD filtering was followed by cell averaging cfar and the output plot is given in Figure 35. The parameters for processing are given in Table 22.

Targets 3 and 4 approach the radar antenna main beam by CPI 6 and continue in that vicinity until CPI10 (again, refer to Figure 32). CREST46 processing results using the three-pulse ADPCA algorithm were able to show the presence of targets 2 and 3. Both the JD and three-pulse ADPCA algorithm, followed by cell averaging CFAR, produced results that resolved both targets. Table 23 gives the parameters used for three-pulse ADPCA processing. The detection map after ADPCA filtering and CFAR processing is shown in Figure 36. As with a previous ADPCA processing example motion compensation was used to account for the small amount of Doppler shift in the main beam clutter.

CPI 7 is the first CPI to show target 4 as well as target 3 and target 2. It is interesting to point out that target 2 is still present although it is outside the main beam by approximately 21° (from boresight). Recall that target returns are not only a function of antenna gain but also radar cross section. As can be seen in Table 19 the target-to-noise
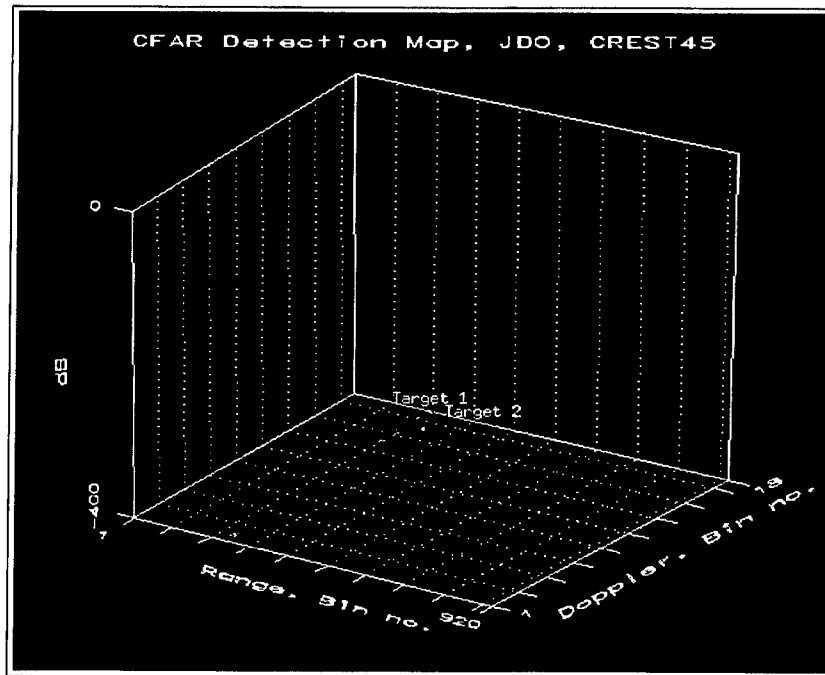
Fig. 35. Joint Domain Processing Followed by Cell Averaging CFAR Performed on CREST45, pfa= 10^{-6}.

Table 23. Adaptive Displaced Phase Center Array Processing, CREST46

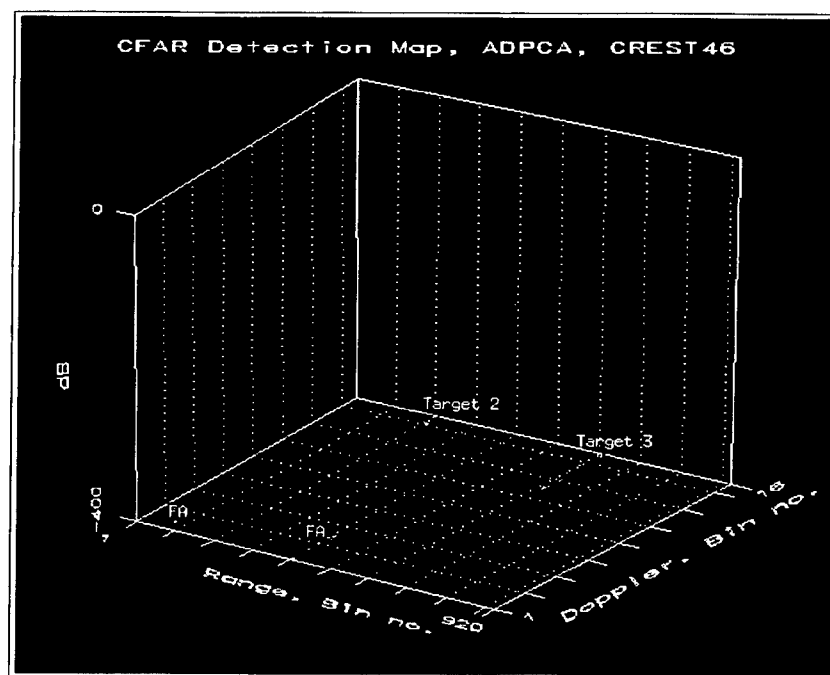| Parameter	Description
pulse compression	LFM(50 μsec, 0.5 MHz), rectangular weight
motion compensation	-8.89 Hz
training range cells (no.)	1 - 800
guard cells (no.)	none
no. of pulses	3
diagonal loading (wrt peak)	-50 dB
steering vector spatial az. weight	Hamming
steering vector spatial el. weight	rectangular
steering vector temporal weight	$[1, -2, -1]$
Doppler filtering	80 dB Chebyshev
CFAR	cell averaging, 40 bins
pfa	10^{-6}

72

Fig. 36. Three-Pulse ADPCA Processing Followed by Cell Averaging CFAR Performed on CREST46, pfa= 10^{-6}.

ratio prior to any processing for target 2 in CPI 7 is large and probably accounts for its presence in detection results for later CPIs.

In order to detect targets 2, 3, and 4 the three-pulse ADPCA algorithm was used again. Table 24 gives the processing parameters for this example. Figure 37 shows the detection map after ADPCA filtering and cell averaging CFAR.

Processing CPI 8 through CPI 10 with all four algorithms described in Section 3 using various training strategies resulted in the detection of target 4 only. The following three tables and three figures document the processing of CPI 8 through CPI 10.

Table 24. Adaptive Displaced Phase Center Array Processing, CREST47

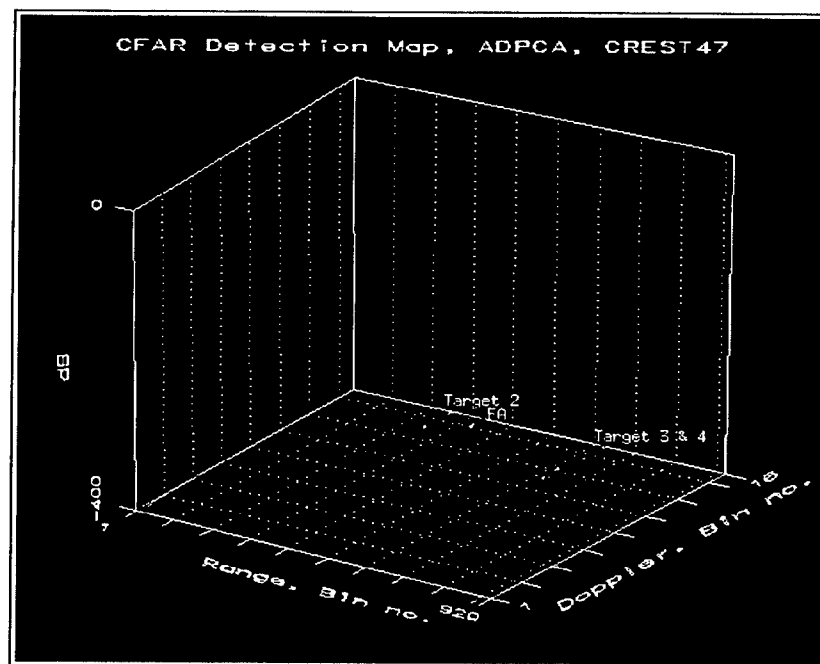| Parameter	Description
pulse compression	LFM(50 μsec, 0.5 MHz), rectangular weight
motion compensation	-26.66 Hz
training range cells (no.)	100 - 800
guard cells (no.)	none
no. of pulses	3
diagonal loading (wrt peak)	-50 dB
steering vector spatial az. weight	Hamming
steering vector spatial el. weight	rectangular
steering vector temporal weight	$[1, -2, -1]$
Doppler filtering	80 dB Chebyshev
CFAR	cell averaging, 40 bins
pfa	10^{-6}

Fig. 37. Three-Pulse ADPCA Processing Followed by Cell Averaging CFAR Performed on CREST47, pfa= 10^{-6}.

74

Table 25. Factored Time Space Processing, CREST48

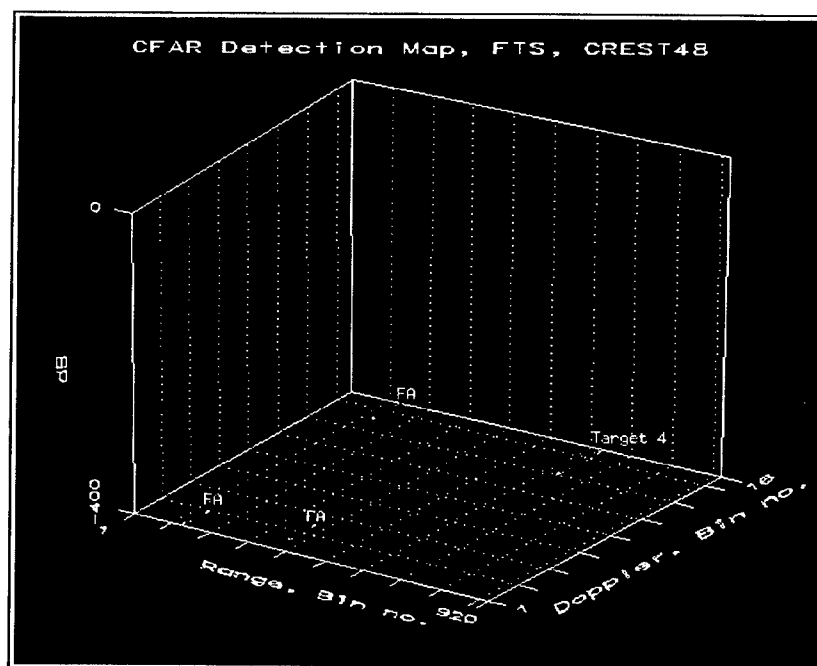| Parameter	Description
pulse compression	LFM(50 μsec, 0.5 MHz), rectangular weight
motion compensation	-44.34 Hz
MTI	3 pulse
training range cells (no.)	100 - 800
guard cells (no.)	none
no. of pulses	3
diagonal loading (wrt peak)	-50 dB
steering vector spatial az. weight	Hamming
steering vector spatial el. weight	rectangular
Doppler filtering	Hamming
CFAR	cell averaging, 40 bins
pfa	10^{-6}

Fig. 38. Factored Time Space Processing Followed by Cell Averaging CFAR Performed on CREST48, pfa= 10^{-6}.

75

Table 26. Joint Domain Processing, CREST49

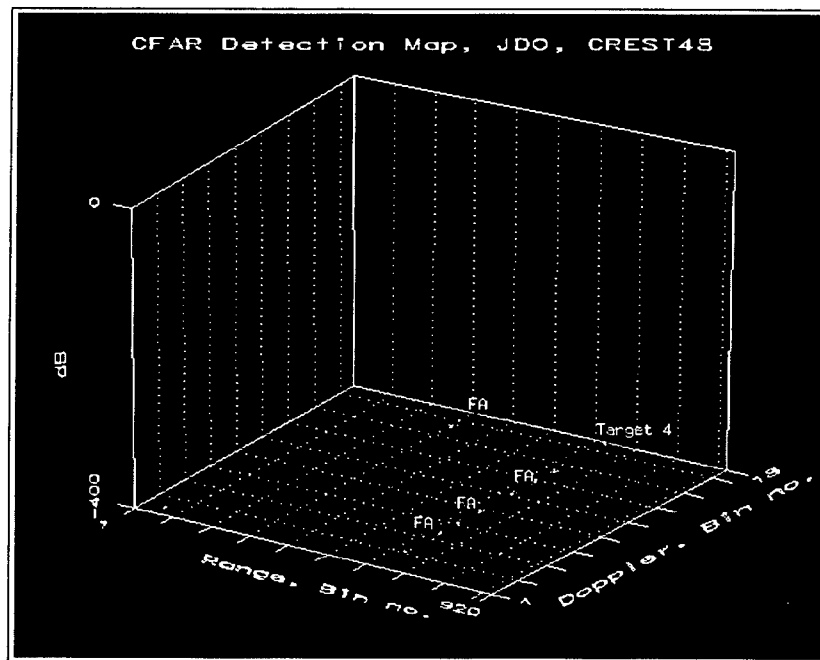| Parameter	Description
pulse compression	LFM(50 μsec, 0.5 MHz), Hamming weight
training range cells (no.)	1 - 850
guard cells (no.)	none
diagonal loading (wrt peak)	-50 dB
steering vector spatial az. weight	Hamming
steering vector spatial el. weight	rectangular
steering vector temporal weight	Hamming
CFAR	cell averaging, 40 bins
pfa	10^{-6}

Fig. 39. Joint Domain Processing Followed by Cell Averaging CFAR Performed on CREST49, pfa= 10^{-6}.

Table 27. Joint Domain Processing, CREST410

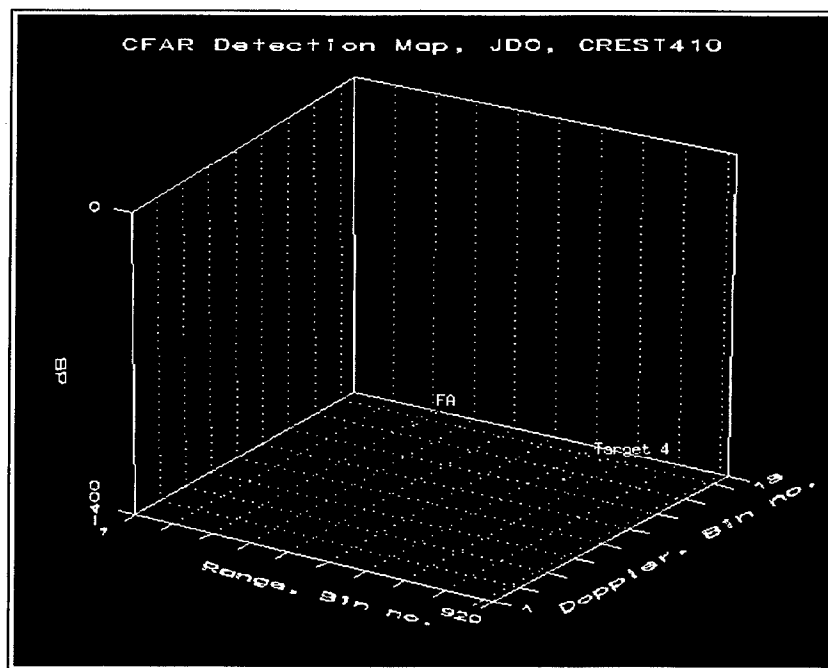| Parameter	Description
pulse compression	LFM(50 μsec, 0.5 MHz), Hamming weight
training range cells (no.)	1 - 850
guard cells (no.)	none
diagonal loading (wrt peak)	-50 dB
steering vector spatial az. weight	Hamming
steering vector spatial el. weight	rectangular
steering vector temporal weight	Hamming
CFAR	cell averaging, 40 bins
pfa	10^{-6}

Fig. 40. Joint Domain Processing Followed by Cell Averaging CFAR Performed on CREST410, pfa= 10^{-6}.

8 Conclusions

This report documents the data sets contained in the DARPA sponsored CREST Challenge. It is believed that the challenge data sets will help support two functions. They will provide a pathway for the novice user of RLSTAP to become more acquainted with the tool. Having documented data sets and analysis results to duplicate will shorten the learning time for new users of RLSTAP.

The data sets also serve as well documented baselines for researchers to test their algorithms in various interference environments and signal scenarios. RLSTAP/ADT is a state of the art software tool which can generate realistic multi-channel radar data from a variety of clutter sites throughout the continental United States. This is a unique feature of RLSTAP and can be used for simulation studies prior to costly flight tests. The data sets in the Challenge are reflective of the kinds of high fidelity clutter and target scenarios that can be generated with RLSTAP/ADT.

More information about the CREST Challenge data sets and the challenge in general can be obtained via the CREST home page on the WWW, wwwcrest.mhpcc.edu. Data sets from the challenge will remain on the web for future download. The most recent version of RLSTAP is also available.

References

[1] Blum, R.S., Melvin, W.L., and Wicks, M.C. An Analysis of Adaptive DPCA. *Proceedings of the IEEE National Radar Conference*, Ann Arbor MI, pp. 303-308, May 1996.

[2] Long, M.W. *Airborne Early Warning System Concepts,* Artech House Inc., MA, 1992.

[3] Marshall, D.F. Evaluation of STAP Training Strategies with Mountaintop Data, *Technical Report MTP-5, Lincoln Laboratory, M.I.T.*, February 21, 1996.

[4] Melvin, W.L. Nonhomogeneity Detection for Adaptive Signal Processing, *Proceedings of the 1996 IASTED International Conference on Signal and Image Processing*, Orlando, FL, November 11-14, 1996.

[5] Michels, J.H. Summary of Space-Time Processing Algorithms, *Internal Rome Laboratory Memo*, July 25, 1995.

[6] Pugh, M.L. and Zulch, P.A. RLSTAP Algorithm Development Tool for Analysis of Advanced Signal Processing Techniques. In *Proceedings of the 29th Asilomar Conference on Signals, Systems, and Computers*, Pacific Grove, CA, November 1995.

[7] Reed, I.S., Mallett, J.D., and Brennan, L.E. Rapid Convergence Rate in Adaptive Arrays. *IEEE Trans. on Aerospace and Electronic Systems*, Vol AES-10, No. 6, pp. 853-863, November 1974.

[8] Rome Laboratory Space-Time Adaptive Processing (RLSTAP) Interface Control Document. *Rome Laboratory html document*, December 1996.

[9] Titi, G.W. An Overview of the ARPA Mountaintop Program. *Proceedings of the IEEE Long Island Section Adaptive Antenna Systems Symposium*, Melville, NY, pp. 53-59, Nov 7-8, 1994.

[10] Ward, J. Space Time Adaptive Processing for Airborne Radar. MIT/LL Technical Report, No. 1015, Lexington, MA, Dec. 1994.

DISTRIBUTION LIST

addresses	number of copies
ATTN: DR. PETER A. ZULCH ROME LABORATORY/OCSA 26 ELECTRONIC PKY ROME, NY 13441-4514	5
ROME LABORATORY/CA CHIEF SCIENTIST 26 ELECTRONIC PKY ROME NY 13441-4514	1
ROME LABORATORY/SUL TECHNICAL LIBRARY 26 ELECTRONIC PKY ROME NY 13441-4514	1
ATTENTION: DTIC-OCC DEFENSE TECHNICAL INFO CENTER 8725 JOHN J. KINGMAN ROAD, STE 0944 FT. BELVOIR, VA 22060-6218	2
ADVANCED RESEARCH PROJECTS AGENCY 3701 NORTH FAIRFAX DRIVE ARLINGTON VA 22203-1714	1
ROME LABORATORY/IMPS 26 ELECTRONIC PKY ROME NY 13441-4514	1
MAJ. DANIEL GAMMON, USAF DARPA 4001 N. FAIRFAX DR., SUITE 500 ARLINGTON, VA 22203	1
DR. JOSEPH GUERCI SAIC/ADT 4001 N. FAIRFAX DR., SUITE 400 ARLINGTON, VA 22203	1

MR. WILL KNAPTON   1
NAVAL RESEARCH LABORATORY
4555 OVERLOOK AVE., SW
WASHINGTON, DC 20375-5336

MR. MICHAEL PICCIOLO   1
NAVAL RESEARCH LABORATORY
4555 OVERLOOK AVE., SW
WASHINGTON, DC 20375-5336

MISSION
OF
ROME LABORATORY

Mission. The mission of Rome Laboratory is to advance the science and technologies of command, control, communications and intelligence and to transition them into systems to meet customer needs. To achieve this, Rome Lab:

a. Conducts vigorous research, development and test programs in all applicable technologies;

b. Transitions technology to current and future systems to improve operational capability, readiness, and supportability;

c. Provides a full range of technical support to Air Force Material Command product centers and other Air Force organizations;

d. Promotes transfer of technology to the private sector;

e. Maintains leading edge technological expertise in the areas of surveillance, communications, command and control, intelligence, reliability science, electro-magnetic technology, photonics, signal processing, and computational science.

The thrust areas of technical competence include: Surveillance, Communications, Command and Control, Intelligence, Signal Processing, Computer Science and Technology, Electromagnetic Technology, Photonics and Reliability Sciences.